

# Sleep-Related Neural Activity in a Premotor and a Basal-Ganglia Pathway of the Songbird

Richard H. R. Hahnloser, Alexay A. Kozhevnikov and Michale S. Fee

*J Neurophysiol* 96:794-812, 2006. First published Feb 22, 2006; doi:10.1152/jn.01064.2005

**You might find this additional information useful...**

---

This article cites 44 articles, 21 of which you can access free at:

<http://jn.physiology.org/cgi/content/full/96/2/794#BIBL>

Updated information and services including high-resolution figures, can be found at:

<http://jn.physiology.org/cgi/content/full/96/2/794>

Additional material and information about *Journal of Neurophysiology* can be found at:

<http://www.the-aps.org/publications/jn>

---

This information is current as of August 14, 2006 .

# Sleep-Related Neural Activity in a Premotor and a Basal-Ganglia Pathway of the Songbird

Richard H. R. Hahnloser,<sup>1,2</sup> Alexay A. Kozhevnikov,<sup>2,3</sup> and Michale S. Fee<sup>2,3</sup>

<sup>1</sup>Institute for Neuroinformatics University of Zurich/Swiss Federal Institute of Technology, Zurich, Switzerland; <sup>2</sup>Bell Labs, Lucent Technologies, Murray Hill, New Jersey; and <sup>3</sup>McGovern Institute for Brain Research, Massachusetts Institute of Technology, Cambridge, Massachusetts

Submitted 11 October 2005; accepted in final form 15 February 2006

**Hahnloser, Richard H. R., Alexay A. Kozhevnikov, and Michale S. Fee.** Sleep-related neural activity in a premotor and a basal-ganglia pathway of the songbird. *J Neurophysiol* 96: 794–812, 2006. First published February 22, 2006; doi:10.1152/jn.01064.2005. During singing, neurons in premotor nucleus RA (robust nucleus of the arcopallium) of the zebra finch produce complex temporal sequences of bursts that are recapitulated during sleep. RA receives input from nucleus HVC via the premotor pathway, and also from the lateral magnocellular nucleus of the anterior nidopallium (LMAN), part of a basal ganglia-related circuit essential for vocal learning. We explore the propagation of sleep-related spike patterns in these two pathways and their influences on RA activity. We promote sleep in head-fixed birds by injections of melatonin and make single-neuron recordings from the three major classes of neurons in HVC: RA-projecting neurons, Area X-projecting neurons, and interneurons. We also record LMAN neurons that project to RA. In paired recordings, spike trains from identified HVC neuron types are strongly coherent with spike trains in RA neurons, whereas LMAN projection neurons on average exhibit only a weak coherency with neurons in HVC and RA. We further examine the relative roles of HVC and LMAN in generating RA burst sequences with reversible inactivation. Lidocaine inactivation of HVC completely abolishes bursting in RA, whereas inactivation of LMAN has no effect on burst rates in RA. In combination, our data suggest that in adult birds, RA burst sequences in sleep are driven via the premotor pathway from HVC. We present a simple generative model of spike trains in HVC, RA, and LMAN neurons that is able to qualitatively reproduce observed coherency functions. We propose that commonly observed coherency peaks at positive and negative time lags are caused by sequentially correlated HVC activity.

## INTRODUCTION

Spiking neural activity in the mammalian and avian brains recorded during awake behavior is often spontaneously replayed during sleep (Dave and Margoliash 2000; Louie 2001; Nadasdy et al. 1999; Wilson and McNaughton 1994). As sleep-related spike trains are very complex, their generation is believed to involve many neuron types and synaptic mechanisms. The songbird robust nucleus of the arcopallium RA is a premotor area (Nottebohm et al. 1976) in which replayed premotor sequences have recently been found (Dave and Margoliash 2000). RA receives motor-related projections from the higher premotor brain area HVC (Nottebohm et al. 1982; Vicario and Nottebohm 1988). During sleep, HVC exhibits sparse burst sequences that are locked to the RA burst se-

quences (Hahnloser et al. 2002), suggesting an important role of the premotor pathway for RA sleep burst generation.

A separate group of song-related brain areas known as the anterior forebrain pathway (AFP) indirectly connects HVC to RA (Okuhata and Saito 1987). Bilateral lesions in areas of the AFP produce profound deficits in vocal learning in juveniles but have little effect on vocal production in adults (Bottjer et al. 1984; Doupe 1993; Scharff and Nottebohm 1991; Sohrabji et al. 1990). Given that part of the song learning process might occur during sleep (Dave and Margoliash 2000; Deregnacourt et al. 2005; Margoliash 2005), it is possible that the output of the AFP, the lateral magnocellular nucleus of the anterior nidopallium (LMAN), might play an important role for sleep burst generation in RA (Abarbanel et al. 2004).

Spiking activity in the premotor pathway and the AFP has been recently studied in an anesthetized preparation (Kimpo et al. 2003). Paired recordings in LMAN and RA showed that spontaneous bursts in RA are preceded either by bursts in HVC or in LMAN. The propagation of correlated bursts from HVC to LMAN may reflect information processing relevant to consolidation of learned vocal patterns. It was suggested that changes in the motor circuit might be controlled during sleep by LMAN-mediated synaptic plasticity in RA (Dave and Margoliash 2000; Doupe et al. 2004).

Here we describe single-neuron recordings of identified neuron pairs in the HVC, RA, and LMAN circuits in a sleeping bird. In combination with reversible pharmacological inactivation of HVC and LMAN, our data suggest that bursts in RA are driven by the synaptic input from HVC and are not driven by input from LMAN.

Part of our data have already been published previously (Fee et al. 2004; Hahnloser et al. 2002). The data and analysis reported here are more extensive with additional recordings from neurons in the AFP, i.e., from HVC neurons projecting to Area X and from LMAN neurons projecting to RA. In our previous study, we analyzed the correlations of burst events in different neuron pairs with a novel conditional correlation technique. Here we are not interested in bursts as much. We analyze spike train correlations by computing coherency functions, which is a useful technique to discount for correlations arising from bursting tendencies of neurons (Kimpo et al. 2003; Thomson and Chave 1991). This different analysis technique, in addition to confirming our previous results, reveals some interesting new features of our data. We present a

Address for reprint requests and other correspondence: R.H.R. Hahnloser, Institute for Neuroinformatics UNIZH/ETHZ, Winterthurerstrasse 190, 8057 Zurich, Switzerland (E-mail: rich@ini.phys.ethz.ch).

The costs of publication of this article were defrayed in part by the payment of page charges. The article must therefore be hereby marked "advertisement" in accordance with 18 U.S.C. Section 1734 solely to indicate this fact.

simple model for these features, explaining the multiple coherency peaks we observe by sequential activity in HVC.

## METHODS

### Electrophysiology

**ANIMALS.** Zebra finches (*Taeniopygia guttata*) were obtained from commercial suppliers (Old Bridge, NJ and Animal Diffusion, Villarimboud, Switzerland). Animals were maintained on a day-night reversed 12-h light cycle to assist in obtaining sleep during daytime experimental sessions. Surgery began approximately at the onset of the night cycle. Birds were anesthetized with 1–3% isoflurane in oxygen and placed in a stereotaxic apparatus (Stellar, Stoelting). The flat anterior portion of the skull was set at an angle of 65° from horizontal and a thin stainless steel plate was mounted to the skull with dental acrylic (Lang Jet Acrylic). A window was made in the inner and outer bone leaflet over nuclei RA, HVC, and Area X (or RA and LMAN) of the right hemisphere. A small hole (~200 μm) was made in the dura over each area and the uncovered brain was protected with 2% low-melting agarose (Sigma). Wound margins were treated with lidocaine gel. The animal was placed in a small foam restraint and placed in the recording apparatus without further anesthesia. In most experiments, the animal was given a single dose (1–10 μg) of melatonin (Sigma) right after surgery, injected subcutaneously in phosphate-buffered saline. Melatonin is known to promote sleep in birds (Hishikawa et al. 1969; Phillips and Berger 1992). In one bird, we used 1 μg and then 2-μg doses for paired recordings of electroencephalographic (EEG) signals and RA neurons, but then switched to 10-μg doses for all subsequent experiments. The only birds to which we did not administer melatonin were two birds used to produce Fig. 2C and two birds in which we recorded RA neuron pairs and RA-HVC<sub>1</sub> neuron pairs. Because the data from the latter two birds were similar to the melatonin-related data, we included them in Fig. 8, B and E. Data were obtained from a total of 50 zebra finches.

**EEG RECORDINGS.** We measure the EEG by differential recording between two electrodes, one placed above the dura near the sagittal sinus, the other placed below the dura ~2 mm lateral and 2 mm anterior of the bifurcation of the sagittal sinus (lambda). Signals were amplified ( $G = 1,000$ ) and filtered (HP > 1 Hz, LP < 100 Hz, DAM-80, WPI).

**SINGLE-UNIT RECORDINGS.** Simultaneous paired and triplet single-unit recordings were made in nucleus RA, HVC, and LMAN. High signal-to-noise (>10:1) recordings were made using sharp glass microelectrodes (5–15 MΩ, borosilicate, 1.0 mm OD, 0.7 mm ID) pulled on a vertical electrode puller (Model 730, Kopf Instruments) and filled with 2 M NaCl. Signals were amplified using Neurodata IR285 (Cygnus Instruments) or Axoclamp-2B (Molecular Devices) intracellular amplifiers. Custom electronics were used for additional amplification (gain of 100) and filtering (300-Hz high-pass 5-pole Bessel filter, 10-kHz low-pass constant delay filter). Extracellular signals were digitized to 16-bit precision at a sampling rate of 20 kHz and stored in blocks of 200 s on a Pentium-based PC running custom Labview software (National Instruments). For triplet recordings, spike signals recorded on a tungsten electrode in RA were amplified using a DAM-80 extracellular amplifier (World Precision Instruments). Single-unit spike trains were confirmed off-line by complete suppression of the spike autocorrelation functions at time lags <1 ms.

**ANTIDROMIC ACTIVATION.** Bipolar stimulating electrodes were placed in RA and/or Area X for antidromic identification of RA-projecting and Area X-projecting HVC neurons, as well as of RA-projecting LMAN neurons. Figure 1. Stimulation electrodes consisted of a pair of Teflon-insulated 50-μm-diam stainless steel wires (California Fine Wire) spaced 0.5 mm apart. For RA stimulation, one electrode was positioned within RA and the other electrode positioned

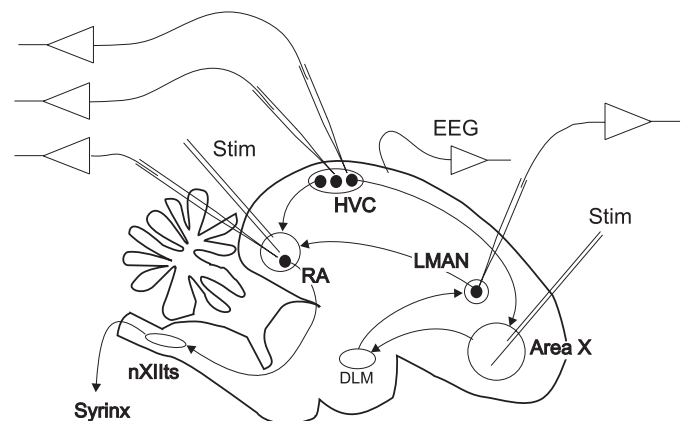


**FIG. 1.** Schematic of the song-control system and experimental setup. Vocal motor neurons in the hypoglossal nucleus (nXIIIts) are innervated by nucleus RA, which in turn receives input from HVC and from lateral magnocellular nucleus of the anterior nidopallium (LMAN). Single-unit recordings were made in 2 premotor song control nuclei (RA and HVC) and in the anterior forebrain nucleus LMAN in awake and sleeping zebra finches. HVC and LMAN neuronal types were identified by antidromic stimulation from nucleus RA and Area X. Electroencephalographic (EEG) signals were recorded to characterize firing patterns in the sleeping state.

more dorsally. For Area X stimulation, both electrodes were placed within Area X. Electrical stimulation was produced using an isolated stimulation unit (AMPI) with intensities in the range 50–500 μA. For most experiments, single monophasic pulses of 0.2-ms duration were used.

HVC neurons were found and isolated using ongoing 1-Hz stimulation in RA or Area X to elicit spike responses. Once a cell was isolated, stimulation threshold current was measured and stimulus intensity was set between 10 and 50% above threshold to produce a reliable response. Continuous analog records were acquired for 60 stimuli at 1-s intervals. The response latency is defined as the interval between stimulus onset and the first evoked spike. Latency variability is defined as the SD of response latencies. Using artificial stimulation responses, we estimate that the contribution to the latency variability due to our fixed sampling rate of 20 kHz is <16 μs.

For some neurons, collision tests were done by stimulating in RA or Area X with some delay after a spontaneous spike. For putative projection neurons, stimulating at small delays (1–3 ms) in the target area resulted in 100% failure of the antidromic spike (collisions). For interneurons, stimulating at small delays did not result in antidromic spike failure ( $n = 10$ ). When putative interneurons were stimulated at delays of 1–2 ms after spontaneous spikes, both average latency and latency variability decreased by 10–15% compared with that resulting from stimulation not triggered on spikes. Hence only a small fraction of the latency variability of putative interneurons can be attributed to activity-related changes in axon conduction velocity (Swadlow 1998).

All RA neurons analyzed in this study are from putative RA projection neurons even though we did not identify RA projection neurons using antidromic stimulation. We believe to have reliably distinguished RA projection neurons from other RA neuron types based on firing statistics and spike waveforms. In comparison to RA projection neurons, RA interneurons exhibit an absence of a regular firing mode in the awake bird, they have unusually high average burst rates in the sleeping bird (>5 bursts/s), and their spike waveforms are significantly narrower (Leonardo and Fee 2005). Note: we frequently recorded from RA neurons with 3–5 MΩ tungsten electrodes, permitting us to clearly observe the narrower spike waveforms in putative RA interneurons. Due to their very infrequent occurrence, RA interneurons were discarded from analysis in this study.

**REVERSIBLE LESIONS IN HVC AND LMAN.** The effect of lidocaine injections in HVC and LMAN on sleep burst rate in RA was examined

by micro-injection of lidocaine (2% in phosphate-buffered saline) during single-unit recordings in RA. Injections were made from pulled glass pipettes (50- $\mu\text{m}$  tip size) using a pressure injection system (Pico Spritzer). Injected volumes were 10–100 nl. Control injections were made in HVC with phosphate-buffered saline. In the LMAN injection experiments, we tested three injection sites; one below, one inside, and one just above LMAN. The anatomical localization of LMAN was done by recording RA-triggered antidromic responses in LMAN prior to insertion of the injection pipette. In the HVC injection experiments, HVC location was verified by recording sleep bursts in HVC interneurons. To measure the effect of the injection in RA, we counted the number of bursts in RA neurons in the minute before and after the injection. Statistical significance of burst-rate differences before and after injection was assessed using the paired *t*-test with a significance level  $P < 0.01$ .

After each experiment, the animal was killed by intramuscular injection of 20% urethan or pentobarbital sodium (Nembutal). The brain was removed for histological examination of unstained slices to verify the location of stimulating and recording electrodes, and drug injection sites. All experiments were carried out in accord with protocols approved by the local IACUC and the Veterinary Office of the Canton of Zurich, Switzerland.

### Data analysis

**INSTANTANEOUS FIRING RATE.** Because of the large dynamic range of firing rates in RA and HVC, spike rasters are not well suited for visualizing long traces of neural activities. Therefore we represented the activity at time  $t$  of a neuron by the instantaneous firing rate  $R(t)$ , a continuous function defined by the inverse of the closest inter-spike interval

$$R(t) = \frac{1}{t_{i+1} - t_i}, \text{ for } t_i < t \leq t_{i+1},$$

where  $t_i$  is the time of the  $i$ th spike.

**BURST RATE.** We identified a group of at least two spikes as a burst if the instantaneous firing rate continuously exceeded 100 Hz. The

burst rate was defined as the number of events per unit time in which the instantaneous firing rate crossed the 100-Hz barrier from below.

**FIRING RATE IN BURST TRAINS.** In Fig. 6, we computed firing rates in burst trains. These spike trains were constructed by removing all single spikes not part of a burst, i.e., all spikes that did not form an interspike interval of  $<100$  ms with another spike. Removing single spikes was particularly effective for RA and  $\text{HVC}_1$  neurons, which produced many single spikes in the awake state and during sleep (Figs. 2 and 4–6).

To measure firing rates also on a coarser temporal scale than by the instantaneous firing rate, we measured the average number of spikes per second  $f$  in nonoverlapping 3-s windows. The histograms of thus measured firing rates are plotted for RA,  $\text{HVC}_1$ ,  $\text{HVC}_{\text{RA}}$ , and  $\text{HVC}_X$  neurons in Fig. 6A. We chose a 3-s window to account for the long tails in the auto-covariance functions in Fig. 5, while still aiming for a local estimate of firing rate. For simultaneously recorded neuron pairs, we reduced the original spike trains to burst trains and computed correlation coefficients between firing rates measured in corresponding 3-s windows, reported as histograms in Fig. 6B. Typically, windows much smaller or larger than 3 s produced weaker correlations and fewer correlated pairs.

For each pair of burst trains, we computed the ratio  $r = \langle f_A \rangle / \langle f_B \rangle$  of average firing rate  $\langle f_A \rangle$  in neuron A and average firing rate  $\langle f_B \rangle$  in neuron B (averaged over all 3-s windows), reported in the histograms in Fig. 6C. Neuron B was always chosen to be the neuron type firing fewer spikes on average. That is, for  $\text{HVC}_{\text{RA}}$ -RA pairs and  $\text{HVC}_{\text{RA}}$ - $\text{HVC}_1$  pairs, neuron B is the  $\text{HVC}_{\text{RA}}$  neuron; for RA- $\text{HVC}_1$  pairs, neuron B is the RA neuron, and for  $\text{HVC}_X$ - $\text{HVC}_1$  pairs, neuron B is the  $\text{HVC}_X$  neuron. Again firing-rate ratios were plotted as  $\blacksquare$  when the firing-rate correlations in Fig. 6B were significant, and they were plotted as  $\square$  when firing-rate correlations were not significant. Due to the large spread and distant outliers of measured ratios, we summarized the histograms of firing-rate ratios by the median value  $r_m$  instead of the mean value (including significantly and nonsignificantly correlated pairs).

By performing the same analysis but without removing single spikes, we observed much smaller firing-rate fluctuations in RA

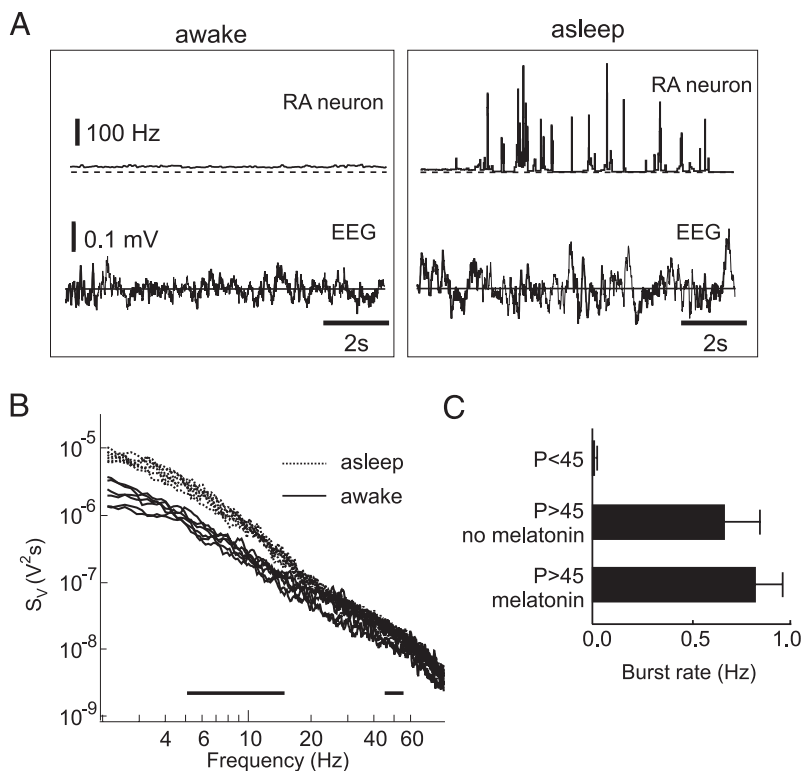


FIG. 2. A: simultaneous recording of the EEG signal and the instantaneous firing rate of an RA neuron in the awake and sleeping state. The dashed lines on top indicate 0-Hz firing rate. B: log-log plot of EEG spectra in the awake and the sleeping states. Based on these curves, we quantified the EEG state by the ratio  $P$  of energy  $S_V$  in a 5- to 15-Hz band to the energy in a 45- to 55-Hz band (horizontal lines). C: average burst rate of RA neurons was almost 0 in the awake state (defined by  $P < 45$ ) and was elevated in the sleeping state ( $P > 45$ ). In 3 birds, the sleep data were collected before and after administering melatonin. With melatonin, the birds spent little time in the awake state, and so the average burst rates in RA were elevated compared with pre-melatonin rates.

and  $HVC_I$  neurons due to their tendency to produce regular spike trains. In general, not removing single spikes in Fig. 6 led to a decreased number of correlated neuron pairs and to a lower degree of correlation. Not removing single spikes in  $HVC_{RA}$  and  $HVC_X$  neurons also led to slightly decreased correlations.

**SPIKE WAVEFORM CLASSIFICATION.** For the HVC spike waveform classification, only waveforms of equal polarity (1st negative, then positive), very large signal-to-noise ratio and small SD were selected (interestingly, for all neurons types, >10% of the recorded spike waveforms had opposite polarity, going positive first). The waveforms shown in Fig. 3E each corresponds to the averages of 25 spontaneous spike waveforms. Only waveforms of single spikes were used to avoid the additional waveform variability associated with bursts. Each of the 25 examples was interpolated at 5- $\mu$ s intervals using the fast Fourier transform, mean-subtracted, normalized to one at the peak, and aligned in time. Spike width was measured at 25% of the peak amplitude.

The nearest waveform classifier that was used to sort spike waveforms associates a waveform to class I if and only if the waveform to which it is closest belongs to class I. This classifier has an advantage over other classifiers such as the perceptron in that it can in principle achieve correct classification even though the geometry of the data are unknown (for example, the data need not be linearly separable).

**INTERSPIKE INTERVAL (ISI) PROBABILITY DENSITY FUNCTION (PDF).** We characterized the spike train of a neuron (labeled A) by the ISI pdf  $h_A(\tau)$  (here  $\tau$  stands for the ISI). First we computed the ISI histogram with bin centers  $\tau_i$  chosen on a logarithmic scale ( $i = 1, \dots, 100$ ). We then derived the ISI pdf  $h_A(\tau_i)$  simply by dividing the ISI histogram by the total area under the histogram, such that  $\sum_i h_A(\tau_i) = 1$ . In essence, the ISI pdf is a normalized ISI histogram. The fact that the ISI pdf sums to one is useful when we average over neurons and when we test spike trains for renewal statistics by means of autocovariance functions.

**AUTO-COVARIANCE FUNCTIONS.** The auto-covariance function  $C_{AA}(t)$  of a spike train  $\rho_A(t)$  (modeled as a sum of delta functions) is a measure of spike rate fluctuations. It is defined as

$$C_{AA}(t) = \frac{1}{T - |t|} \int_0^T \rho_A(s+t) \rho_A(s) ds - \bar{\rho}_A^2 \quad (1)$$

where  $\bar{\rho}_A$  is the mean firing rate of neuron A over the entire recording, and  $T$  is the duration of the recording (the denominator  $T - |t|$  results in an unbiased estimation of auto-covariance at large times  $t$  after setting  $\rho_A(t) = 0$  for  $t < 0$  and  $t > T$ ). The first term on the right side of Eq. 1 is known as the auto-correlation function. By subtracting the term  $\bar{\rho}_A^2$  from the auto-correlation function, the asymptotic value of the

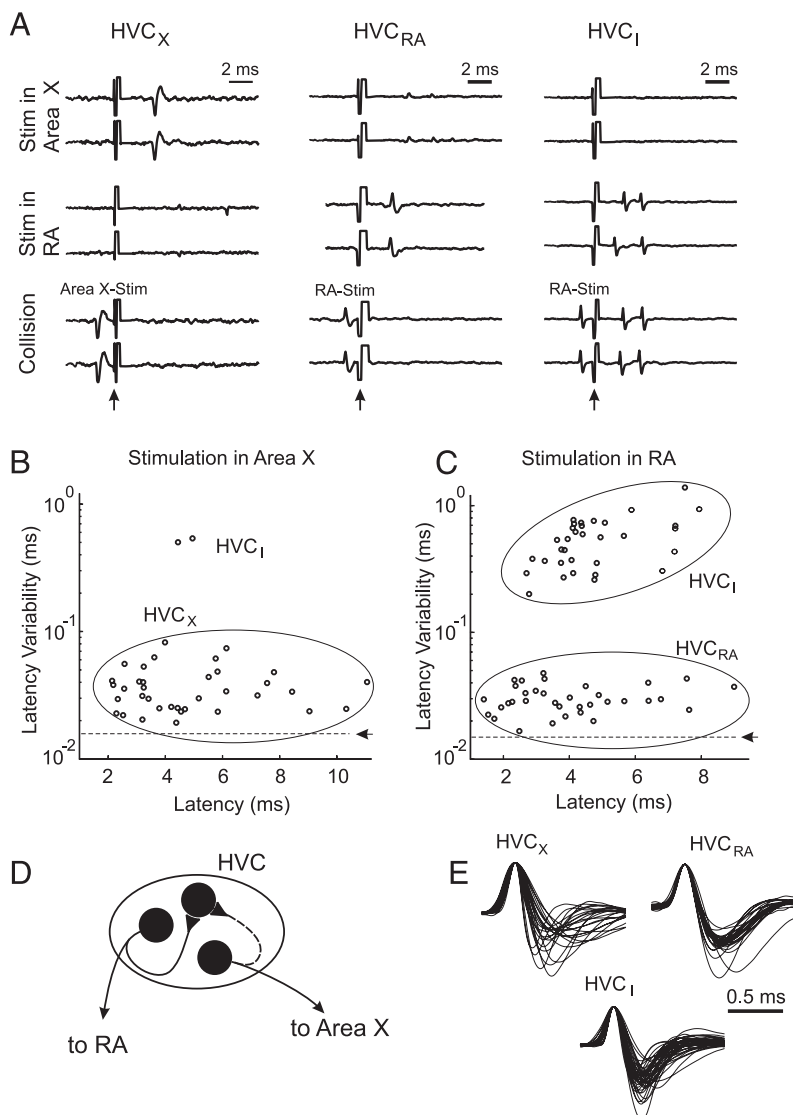


FIG. 3. A: single-unit responses of three types of HVC neurons. On the left, the  $HVC_X$  neuron responded to electrical stimulation in Area X, but not to stimulation in RA. In the middle, the  $HVC_{RA}$  neuron responded to stimulation in RA, but not in Area X. On the right, the  $HVC_I$  neuron responded to stimulation in RA, but not in Area X. The bottom row shows results from a collision test. Stimulation in Area X immediately after a spontaneous spike in the  $HVC_X$  neuron resulted in collision with the antidromic spike. Likewise, stimulation in RA following a spontaneous spike in the  $HVC_{RA}$  neuron resulted in collision there. In contrast, no collision resulted from RA stimulation following spontaneous spikes in the  $HVC_I$  neuron. The vertical arrows indicate the stimulation artifacts. B: scatter plot of antidromic spike latency versus latency variability for  $HVC_X$  neurons; these neurons responded with a small average latency variability of 30  $\mu$ s. C:  $HVC_{RA}$  neurons responded with a latency variability of 20–60  $\mu$ s to RA stimulation, while  $HVC_I$  neurons responded with approximately 300–1000  $\mu$ s latency variability. The dashed horizontal line in B and C represents the noise level associated with A/D sampling errors. D: schematic illustrating the proposed circuitry. The strong asymmetry in activation of  $HVC_I$  neurons suggests that  $HVC_{RA}$  neurons activate  $HVC_I$  neurons more effectively than do  $HVC_X$  neurons. E: average spike waveforms for 24  $HVC_X$  neurons, 30  $HVC_{RA}$  neurons, and 46  $HVC_I$  neurons. Within-class variability prevented reliable classification of neuron type based on spike waveform.

auto-covariance function is zero. For better visibility, results in the figures are plotted on a logarithmic scale  $t_i$  by integration between adjacent points, i.e., shown is the discrete function  $C_{AA}(i) = \int_{t_i}^{t_{i+1}} C_{AA}(t) dt$ . In Figs. 5*F* and 11*D*, we have plotted the average auto-covariance functions  $\langle C_{AA}(t) \rangle_A$  by averaging over all neurons *A* of the same type.

A simple test of the complexity of a spike train is to probe it for renewal statistics, i.e., to test whether the spike train is generated by randomly drawing interspike intervals from the ISI pdf (Cox 1962). This test assumes that interspike intervals occur in completely random order and with a frequency set solely by the ISI pdf. Spike trains often do not form renewal processes, which may benefit their coding abilities (Holden 2004). To perform renewal tests on our spike trains, we computed renewal auto-covariance function  $C_{AA}^R(t)$  for each neuron. In the frequency domain, the renewal auto-covariance function  $C_{AA}^R(\omega)$  can be derived from the ISI pdf  $h_A(\tau)$

$$C_{AA}^R(\omega) = \bar{\rho}_A \operatorname{Re} \left[ \frac{1 + h_A(\omega)}{1 - h_A(\omega)} \right] - \bar{\rho}_A^2 \quad (2)$$

where  $h_A(\omega)$  is the Fourier transformed ISI pdf and  $\operatorname{Re}$  denotes the real part of a complex number. For a derivation of Eq. 2 see e.g., (Gerstner and Kistler 2002). Any deviation of  $C_{AA}(t)$  from  $C_{AA}^R(t)$  is indicative of a memory in the spike train that causes the occurrence of a particular ISI to be conditional on previous ISIs. We tested differences between the two functions for significance by the Jackknife variance estimator (for details on the Jackknife, see SIGNIFICANCE OF COHERENCY FUNCTIONS). Average renewal functions  $\langle C_{AA}^R(t) \rangle_A$  were computed by averaging over individual renewal functions and were plotted as dashed lines in Figs. 5*F* and 11*D*.

**COHERENCY ANALYSIS.** In addition to slow correlations of firing rates analyzed in 3-s windows, we quantified fast correlations between spike trains in simultaneously recorded cells by the coherency function  $\gamma_{AB}(t)$ . The coherency function is similar to the cross-covariance function; we computed it as follows. First we computed the cross-covariance function  $C_{AB}(t)$  between spike trains  $\rho_A(t)$  and  $\rho_B(t)$  (each modeled as a sum of delta functions)

$$C_{AB}(t) = \frac{1}{T - |t|} \int_0^T \rho_A(s+t) \rho_B(s) ds - \bar{\rho}_A \bar{\rho}_B \quad (3)$$

From the cross-covariance function, the coherency function  $\gamma_{AB}(\omega)$  in the frequency domain was computed by Fourier transformation and normalization

$$\gamma_{AB}(\omega) = \frac{C_{AB}(\omega)}{\sqrt{C_{AA}(\omega) C_{BB}(\omega)}} \quad (4)$$

where  $C_{AA}(t)$  and  $C_{BB}(t)$  are the auto-covariance functions of the spike trains. For convenience, the coherency functions  $\gamma_{AB}(t)$  in Figs. 7–9, 12, and 13 were all plotted in the time domain, by inverse Fourier transformation of  $\gamma_{AB}(\omega)$ . Smoothing of coherency functions  $\gamma_{AB}(t)$  was done by convolution with a Gaussian windowing function of SD of 4 ms. Note that coherency functions were computed at the temporal resolution of data samples, which is 50  $\mu$ s. However, in the figures, coherency functions were plotted at a resolution of 1 ms, which was achieved by summing over coherencies in 1-ms bins. Deliberately, to obtain precise estimates of peak coherency time lags, we chose a smaller time bin for our analysis than the 10-ms bin in Kimpo et al. Note: when we computed coherency functions at a temporal resolution of 10 ms, we found qualitatively similar results as shown in Figs. 7–9, 12, and 13.

We also plotted average coherency functions  $\langle \gamma_{AB}(t) \rangle_{AB}$  for the different neuron types in Figs. 8, 9, *B* and *D*, and 12, *B* and *C*, where the average runs over all neuron pairs of the same types. Plotted in these figures is also the SD of individual coherency functions and the average significance threshold.

**SIGNIFICANCE OF COHERENCY FUNCTIONS.** The significance threshold of the coherency function for a particular neuron pair was assessed by Jackknifing the data in 20 s data windows and computing the Jackknife variance (Thomson and Chave 1991)

$$\sigma_j^2(t) = \frac{N-1}{N} \sum_{i=1}^N (\gamma_{AB}^i(t) - \bar{\gamma}_{AB}(t))^2$$

where  $N$  represents the number of data windows (depending on the duration of the recording),  $\gamma_{AB}^i(t)$  is the coherency function of the jackknifed data with the  $i$ th window missing, and  $\bar{\gamma}_{AB}(t) = \langle \gamma_{AB}^i(t) \rangle_i$  is the average jackknifed coherency function. Note that we used long 20-s windows because of the small firing rates in HVC projection neurons and because all our recordings were  $>200$  s (typical 400–600 s). We set the significance threshold of measured coherencies to three SDs,  $3\sqrt{\sigma_j(t)}$ , shown by dashed lines in Figs. 7, *A–C*, and 9, *A* and *C*. This significance threshold corresponds to a roughly 99% confidence in significance testing. Whenever the coherency function exceeded the significance threshold, a peak emerged. The distributions of peak coherency amplitudes versus peak latencies are shown in the summary plots beneath the average coherency functions in Figs. 8, 9, *B* and *D*, and 12, *B* and *C*. In these figures, we plotted the average significance thresholds of all neuron pairs of the same types as dashed lines.

**NOTE ON COHERENCY ANALYSIS.** Even though our confidence threshold is high (99%) and the jackknife is a highly conservative estimator (Thomson and Chave 1991), we observed many coherency peaks at large time lags ( $t > 100$  ms). Presumably, these peaks arose from correlated fluctuations in firing rates as seen in most neuron pairs (see e.g., Fig. 6). In general terms, whenever data derive from experiments using externally controlled trials, it is possible to account for stimulus-driven fluctuations of firing rates by replacing the average firing rates  $\bar{\rho}_A$  and  $\bar{\rho}_B$  in Eq. 3 by time-dependent trial averages. However, as there are no trials in our experiments, and as we did not have any control over nonstationarities of sleep-related spike trains, there is no simple way of separating correlated fluctuations on a long time scale from fast correlations on a shorter time scale. Our simple solution to this problem was thus to plot all significant coherency peaks in the *bottom parts* of Figs. 8, 9, *B* and *D* and 12, *B* and *C*. The largest peaks were plotted as  $\bullet$ , and secondary peaks were plotted as  $\circ$ . Most often, the largest peaks were found close to zero time lag, whereas the secondary peaks were found at larger positive or negative time lags. This behavior was clearly visible for coherency functions involving HVC<sub>1</sub> neurons such as in Fig. 8, *D* and *E*.

We realize that our choice of using coherency functions as our main analysis tool is a tradeoff: coherencies have the advantage of being a proven standard and allowing for comparison with previous studies but might not be the optimal measure when data are nonstationary and firing rates in different neuron types highly variable.

**SINGLE SPIKES AND RASTER PLOTS.** In our previous report (Hahnloser et al. 2002), we removed single spikes from RA and HVC<sub>1</sub> neuron spike trains for the raster plots and for the correlation analysis (single spikes are those spikes not part of a burst as defined in the preceding text). Here we included all spikes of all neurons; therefore raster plots as in Fig. 7*A* look qualitatively different from those in Fig. 3 of Hahnloser et al. (2002).

**MARKOV MODEL OF SERIAL CORRELATIONS IN HVC, RA, AND LMAN.** The Markov model of HVC, RA, and LMAN spike trains is based on sequential dynamics in two populations of HVC<sub>RA</sub> and HVC<sub>X</sub> neurons. The HVC sleep-burst epochs in the HVC<sub>RA</sub>–HVC<sub>X</sub> populations were modeled as follows: if  $S_t$  is the event that the sleep-burst epoch reaches time  $t$ , then the probability that it also reaches time  $t + 40$  ms is given by  $P(S_{t+40\text{ms}} | S_t) = P(\text{HVC}_X) = 0.8$ . It follows that since its initialization at time  $t$ , the HVC sequence progresses for  $n$  steps up to time  $t + 40n$  ms with probability  $0.8^n$ .

We modeled bursts in  $HVC_I$ ,  $HVC_{RA}$ , RA, and  $LMAN_{RA}$  neurons at fixed delays of these 40-ms intervals. To translate burst times into spike trains (Fig. 13C), we added spikes to the burst onset times as follows: for each burst, first we randomly drew the number  $n$  of spikes from an exponential distribution (rounding the result toward infinity). The mean number of spikes per burst was three for the HVC neuron and the RA neuron, whereas it was two for the  $LMAN_{RA}$  neuron. For each burst, the interspike intervals  $s_i$  were determined by  $s_i = 1 + 0.5r_i^2$  ms ( $i = 1, \dots, n$ ), where  $r_i$  is a random variable drawn from a Gaussian distribution with zero mean and 1 ms<sup>2</sup> variance. The coherency analysis for the artificial spike trains was performed using the same Matlab scripts (Mathworks) as for the natural spike trains except that final coherency functions in Fig. 13 were smoothed with a Gaussian window of 10 ms (instead of 4 ms).

## RESULTS

To examine the origins of sleep-related burst sequences in RA, we have developed a head-fixed sleeping bird preparation that permitted us to perform experiments that would not presently be feasible with chronic recording in the singing bird. Although it is unlikely that a head-fixed bird could be induced to sing, we found that head-fixed zebra finches sleep a significant fraction of the time. Our preparation permits us both to record simultaneously from multiple antidromically identified neurons in several brain areas and to perform reversible lesions by pressure injection of pharmacological agents.

### *Relationship between sleep bursts and EEG*

Sleep and wakefulness in freely behaving birds can be quantitatively distinguished on the basis of spectral content of the EEG at low frequencies (1–30 Hz) (Amlaner and Ball 1994; Nick and Konishi 2001). We found that in the awake head-fixed bird, EEGs consist of a broadband noisy signal falling off at higher frequencies as  $f^{-2}$  (where  $f$  is the frequency, Fig. 2B). During sleep, however, the EEG signal made large low-frequency excursions, corresponding to roughly a factor of 2 more power in a band from 1 to 15 Hz; >20 Hz, the awake and sleeping EEGs were nearly identical, Fig. 2B. These spectral characteristics of head-fixed zebra finches are in agreement with earlier more exhaustive EEG measurements of slow-wave or quiet sleep in the freely behaving pigeon (Tobler and Borbely 1988). We have quantified the spectral differences between sleep and wakefulness by the ratio of energy in the 5- to 15-Hz band to energy in the 45- to 55-Hz band; in the awake state, this ratio was typically  $33 \pm$  (SD) 14 and in the sleeping state the ratio was  $63 \pm 14$  (from 72 1-min records in 3 birds). The sleep EEG state was usually associated behaviorally with closed eyes. However, in one of three birds, sleep-like EEG signals were occasionally observed with the ipsilateral eye open.

In the awake (nonsinging) bird, RA neurons have a regular and tonic activity of low firing rate (Yu and Margoliash 1996). In brain slices, they behave remarkably like integrate-and-fire neurons with no intrinsic bursting tendencies (Mooney 1992). During singing and sleeping, these neurons produce spontaneous bursts of spikes (Dave and Margoliash 2000; Hahnloser et al. 2002). We found that sleep EEGs were strongly associated with the presence of high-frequency spike bursts in RA neurons. In three birds, 35 RA neurons were recorded simultaneously with the EEG; sleep bursts in RA tended to cluster in 1- to 2-s epochs, each comprised of 2–10 bursts. Average RA

burst rate in the sleep EEG state was  $0.67 \pm 0.46$  bursts/s (Fig. 2C) and in the awake EEG state was  $<0.01 \pm 0.01$  bursts/s. Consistent with this observation, in chronic recordings from freely behaving zebra finches, bursts in RA neurons are never observed in awake, nonvocalizing animals (Leonardo and Fee 2005).

Because bursts in RA neurons occurred only during the sleep EEG state, we used the presence of bursts in RA as an operational assay of the sleep state. We did not find any differences in the EEG signal between normal and melatonin-induced sleep. In addition, there was no melatonin dependence of RA burst rates during epochs of sleep EEG state (Fig. 2C). However, after melatonin injection, we consistently observed a ~50% increase in the average burst rate of RA neurons, suggesting that the fraction of time spent sleeping is increased by administering melatonin prior to the experiment.

### *Classification of HVC neurons*

In the following, we provide a detailed electrophysiological analysis of different neuron types in HVC, RA, and LMAN. Our goal was to obtain new insights into their differential contributions to sleep bursts in RA and into the general physiology of sleep in these areas. We first describe results from single neuron recordings, then from recordings in pairs of RA and identified HVC neurons.

Three broad classes of neurons have been previously identified in HVC: RA-projecting neurons ( $HVC_{RA}$ ), Area X-projecting neurons ( $HVC_X$ ), and local interneurons ( $HVC_I$ ). These neuronal populations have distinctive morphological and electrophysiological properties (Dutar et al. 1998; Kubota and Taniguchi 1998). RA-projecting HVC neurons are excitatory and ramify widely in RA (Mooney 2000; Stark and Perkel 1999). Interneurons are spiny (Dutar et al. 1998; Mooney 2000) and inhibitory (Rosen and Mooney 2003). Area X-projecting HVC neurons are spiny and excitatory, just like RA-projecting cells, but they have larger somas and dendritic extension than RA-projecting cells (Dutar et al. 1998).

To identify these neuron types in extracellular recordings, we antidromically activated HVC neurons by electrical stimulation in Area X and in RA. For the purpose of classifying antidromic responses of HVC neurons, high signal-to-noise extracellular recordings were made from 98 neurons in 11 awake and sleeping head-fixed zebra finches. In six birds, stimulating electrodes were placed either in RA ( $n = 3$  birds) or in Area X ( $n = 3$  birds), and in five birds stimulating electrodes were placed in both areas. We identified three distinct response patterns to RA and Area X stimulation (Fig. 3A). Putative Area X-projecting neurons ( $n = 35$ ) responded to low-intensity stimulation (50–500  $\mu$ A) in Area X but did not respond to even high-intensity stimulation ( $\leq 10$  mA) in RA. Near-threshold stimulation produced latencies to the first spike between 2 and 11 ms (average  $4.9 \pm 2.4$  ms) with small latency variability in the range 23–94  $\mu$ s ( $43 \pm 12$   $\mu$ s, Fig. 3B). Putative RA-projecting neurons ( $n = 35$ ) responded to low-intensity stimulation in RA, but did not respond to even high-intensity stimulation in Area X ( $\leq 10$  mA). These neurons responded with only one or two spikes even at high stimulus intensity. Near-threshold stimulation produced latencies to the first spike of 2 to 8 ms (mean  $4.6 \pm 2.4$  ms) and a small latency variability in the range 1–52  $\mu$ s ( $34 \pm 7$   $\mu$ s). Putative HVC

interneurons ( $n = 28$ ) responded to low-intensity stimulation in RA with latencies to the first spike of  $4.4 \pm 1.1$  ms and large latency variability in the range 220–1530  $\mu$ s ( $580 \pm 120$   $\mu$ s, Fig. 3C). Near stimulus threshold these neurons responded with one or two spikes; higher intensities resulted in increased numbers of evoked spikes (in some cases,  $\leq 10$  spikes could be evoked). We found only three examples of putative HVC interneurons that responded to stimulation in Area X.

On the basis of these results, we infer that the putative projection neurons were antidromically activated from their target areas and thus are likely to be HVC<sub>X</sub> neurons and HVC<sub>RA</sub> neurons, respectively (Fig. 3D). In contrast, the non-antidromically activated neurons were likely to be synaptically activated, and we tentatively identify these as HVC<sub>I</sub> neurons.

We did not find significant differences in the extracellular spike waveforms of the three types of HVC neurons when recorded with sharp glass electrodes. Spike widths of HVC<sub>I</sub> neurons [ $0.21 \pm 0.03$  (SD) ms, range: 0.11–0.29 ms,  $n = 80$ ] were slightly (but not significantly) smaller than those of HVC<sub>RA</sub> neurons ( $0.27 \pm 0.04$  ms, range: 0.15–0.38 ms,  $n = 46$ ) and slightly (but not significantly) smaller than those of HVC<sub>X</sub> neurons ( $0.25 \pm 0.05$  ms, range: 0.16–0.38 ms,  $n = 42$ ). The large within-class variability of spike waveforms made a correct classification of neuron type based on waveform difficult: a nearest waveform classifier (see METHODS) misclassified the neurons in  $\sim 20\%$  of cases. Also, none of the classes could be linearly separated from the other two classes with an error rate  $< 20\%$ . Linear separability was based on the

first three principal components of waveform shapes, which described  $> 97\%$  of waveform variability.

In the subsequent experiments, we identified each recorded HVC cell by its antidromic stimulation response, distinguishing HVC<sub>I</sub> neurons from HVC projection neurons by their large differences in spike-latency variability. Nonstimulated cells are not identifiable and thus were not recorded.

#### Firing characteristics of different HVC, RA, and LMAN neuron types

The three neuron types in HVC differed considerably in their spontaneous firing patterns in the awake bird. HVC<sub>X</sub> neurons produced single spikes at a rate of  $1.5 \pm 1.2$  (SD) spike/s. HVC<sub>RA</sub> neurons were not spontaneously active in the awake bird ( $< 0.1$  spike/m). Only HVC<sub>I</sub> neurons exhibited a considerable spontaneous activity in the awake bird of  $7.2 \pm 7.0$  spike/s, in the range of 2–26 spike/s, Fig. 4, A and B.

With the exception of HVC<sub>X</sub> neurons, the firing rates of all HVC neuron types increased significantly during sleep. The main characteristic of sleep-related spike trains in HVC and RA was the emergence of high-frequency bursts.

We characterized spike trains by their interspike-interval (ISI) histograms. To average the histograms for many neurons of the same type, we normalized the histograms by their sum before averaging, resulting in estimates of ISI probability density functions (pdfs), Fig. 4C (see METHODS). RA neurons exhibited a bimodal ISI pdf, with a relatively small peak at 4 ms and a larger peak at  $\sim 50$  ms. The small ISI peak is

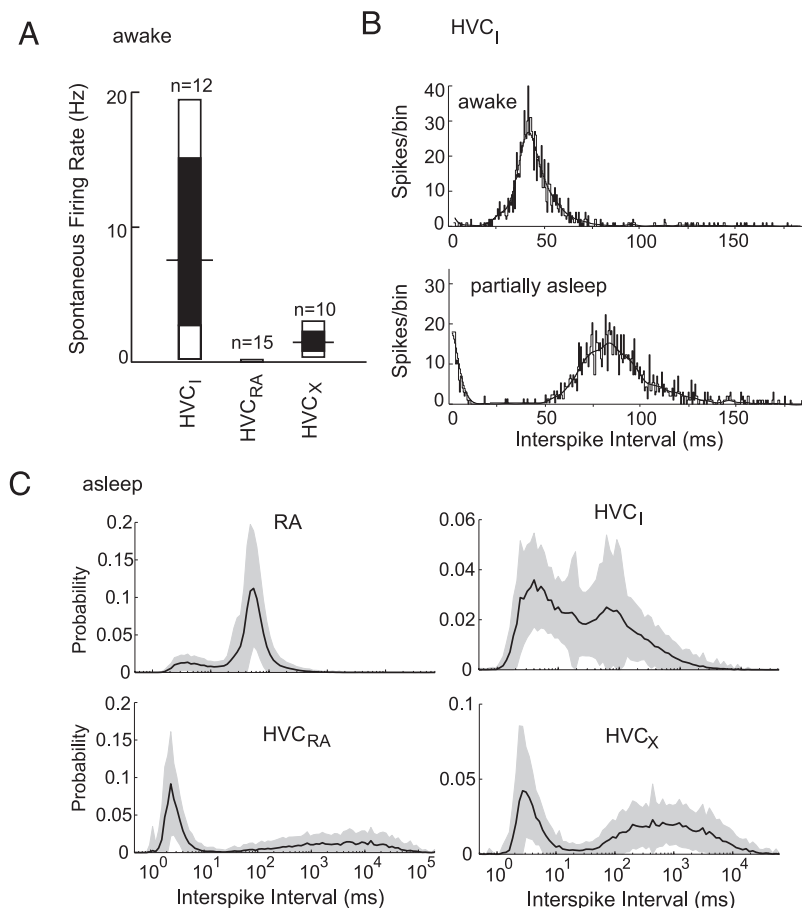


FIG. 4. Activity in HVC neurons of awake and sleeping birds. A: in the awake state, HVC<sub>I</sub> neurons exhibited a wide range of regular firing rates from 0 to 20 Hz with an average of  $\sim 7$  Hz. HVC<sub>RA</sub> neurons were not spiking in the awake bird and HVC<sub>X</sub> neurons typically had a spontaneous activity of 1–2 spikes/s. None of the HVC neuron types burst in the awake bird. B: interspike interval (ISI) histograms for 2 HVC<sub>I</sub> neurons. Top: interneuron in the awake state, firing spikes at interspike intervals of typically 40 ms. Bottom: ISI histogram of an HVC<sub>I</sub> neuron for a bird that slept for a small part of the time during which the data were taken. Notice the appearance of very short interspike intervals. C: average ISI probability density functions (pdf) of identified HVC neurons and of RA neurons during sleep.  $\square$ , SDs of the pdfs. All neuron types exhibited frequent bursting activity that can be seen by the peaks at 3–4 ms.

reminiscent of firing statistics of RA projection neurons during singing (Leonardo and Fee 2005). The latter peak is descriptive of ISIs in awake, nonsinging birds (the average RA neuron firing rate in the awake bird is 15–25 Hz). In combination, ISI pdfs of RA neurons suggest that sleep-related spike trains in RA neurons are a mixture of spike trains during waking and singing.

The average ISI pdf of HVC<sub>1</sub> neurons also exhibited two peaks, although the large ISI peak was smaller than the corresponding peak of RA neurons. This reduced peak is in agreement with a smaller average firing rate of HVC<sub>1</sub> neurons during waking compared with RA neurons.

The average ISI pdf of HVC<sub>RA</sub> neurons exhibited a narrow peak at ~3 ms due to high-frequency bursts, and a very small and broad peak at ~8 s, corresponding roughly to their typical interburst interval (see also Table 1). HVC<sub>X</sub> neurons also exhibited a burst peak at ~3 ms and a broader peak at several hundreds of milliseconds. The latter peak occurred at ISIs one order of magnitude smaller than the second peak of HVC<sub>RA</sub> neurons. This reduced probability of HVC<sub>X</sub> neurons to generate very large ISIs reflects the tendency of HVC<sub>X</sub> neurons to produce more single spikes than do the HVC<sub>RA</sub> neurons (see also Table 1).

The bursts of HVC<sub>1</sub> neurons and of RA neurons tended not to be evenly distributed but were grouped into epochs of increased density, Fig. 5. In recordings of HVC<sub>1</sub> neuron pairs, we found a remarkable co-occurrence of high-density burst epochs marked by black horizontal bars in Fig. 5A. Also on a much smaller time scale, there was abundance of precisely synchronized bursts, Fig. 5B. The two time scales of synchrony between HVC<sub>1</sub> neuron pairs could be clearly seen in cross-covariance functions that had a pronounced peak at zero time lag and a long tail of several seconds before decaying to zero, Fig. 5C. Also in pairs of HVC<sub>1</sub> and RA neurons we observed similar co-occurrence of burst epochs, Fig. 5D. On a smaller time scale, we found that within a burst epoch, many HVC<sub>1</sub> neuron spikes tended to precede RA neuron spikes by a few milliseconds, Fig. 5E. By removing single spikes from the spike trains in Fig. 5E (resulting in what we call burst trains, see METHODS), we found that strong spike correlations remained clearly visible in burst trains.

In the following, we characterize the burst generation mechanisms in the various neuron types and their tendencies to form sleep-burst epochs by close inspection of auto-covariance functions. The average auto-covariance functions of RA and HVC<sub>1</sub> neurons reflected sleep burst epochs by their long tails of over a second, Fig. 5F (top). Note, the oscillatory appearance for auto-covariance functions of RA neurons is due to the awake-like firing mode of these neurons in between burst epochs. Auto-covariance functions of HVC projection neurons did not have long tails and fell to zero within <50 ms, Fig. 5F

(bottom), suggesting the absence of sleep-burst epochs in these neurons. Auto-covariance functions of individual HVC projection neurons were often oscillatory on a small time scale (Fig. 5F, bottom, insets), illustrating their stereotyped bursting behavior.

To learn more about burst generation mechanisms in the different neuron types, we performed renewal tests of their spike trains (Cox 1962). A renewal spike train is said to have no memory because each ISI is a random variable that is independent of previous ISIs. We computed auto-covariance functions for each spike train under renewal assumptions (see METHODS). Deviations from the true auto-covariance functions are indicated by thick horizontal bars in Fig. 5F. Of the 196 RA neurons tested, 20 exhibited nonrenewal auto-covariance functions (Jackknife,  $P < 0.001$ ). Of the 160 HVC<sub>1</sub> neurons tested, 18 exhibited nonrenewal auto-covariance functions (Jackknife,  $P < 0.001$ ). Of the 152 HVC<sub>RA</sub> neurons tested, 34 exhibited nonrenewal auto-covariance functions (Jackknife,  $P < 0.001$ ). And of the 83 HVC<sub>X</sub> neurons tested, 3 exhibited nonrenewal auto-covariance functions (Jackknife,  $P < 0.001$ ).

On a population level, most neuron types displayed nonrenewal statistics. The median auto-covariance function of RA neurons was larger than the median renewal function in the intervals 5–39 ms and 250 ms to 6.9 s (Mann-Whitney rank sum test,  $P < 0.001$ , Fig. 5F). The median auto-covariance function of HVC<sub>1</sub> neurons was larger than the median renewal function in the interval 5 ms to 2.9 s (Mann-Whitney rank sum test,  $P < 0.001$ , Fig. 5F). The median auto-covariance function of HVC<sub>RA</sub> neurons was smaller than the median renewal function in the interval 8–30 ms (Mann-Whitney rank sum test,  $P < 0.001$ , Fig. 5F). However, no where was the median auto-covariance function of HVC<sub>X</sub> neurons significantly different from the median renewal function (Mann-Whitney rank sum test,  $P < 0.001$ , Fig. 5F). In conclusion, whereas RA and HVC<sub>1</sub> neurons tended to have broader auto-covariance functions than expected by renewal statistics, those of HVC<sub>RA</sub> neurons tended to be narrower. This means that HVC<sub>RA</sub> neurons are subject to some sort of fatigue or adaptation that prevents them from producing long bursts, whereas RA and HVC<sub>1</sub> neurons are subject to transient reinforcement of increased spike rates. These observations agree well with in vitro findings of spike adaptation in HVC<sub>RA</sub> neurons but not in HVC<sub>1</sub> neurons (Dutar et al. 1998).

We visualized the fluctuations of firing rates during sleep-burst epochs by histograms of firing rates measured in 3-s windows, Fig. 6A. Typically, the histograms extended from large values down to zero firing rate, illustrating the large fluctuations in spike rates on this 3-s time scale. As this analysis does not distinguish between spikes fired in bursts and spikes fired in the awake-like regular mode and because the occurrence of spike bursts was the most prominent difference

TABLE 1. Firing Statistics for various neuron types in sleeping birds

Neuron Type	Firing Rate, s <sup>-1</sup>	Burst Firing Rate, s <sup>-1</sup>	Burst Rate, s <sup>-1</sup>	Burst Width, ms	Spikes/Burst	Spikes In Bursts, %
RA (n = 196)	18 ± 5.4	254 ± 45	0.89 ± 0.53	11.5 ± 3.2	3.5 ± 0.75	18 ± 13
HVC <sub>RA</sub> (n = 152)	0.49 ± 0.62	343 ± 80	0.10 ± 0.13	6.4 ± 1.8	3.1 ± 0.76	73 ± 21
HVC <sub>1</sub> (n = 160)	15.0 ± 9.0	243 ± 46	2.1 ± 1.5	14 ± 4.1	4.0 ± 1.1	53 ± 21
HVC <sub>X</sub> (n = 83)	1.6 ± 1.5	271 ± 57	0.13 ± 0.10	8.4 ± 2.4	3.1 ± 0.55	47 ± 21
LMAN <sub>RA</sub> (n = 29)	3.4 ± 3.2	201 ± 33	0.15 ± 0.20	8.1 ± 1.1	2.5 ± 0.3	13 ± 6

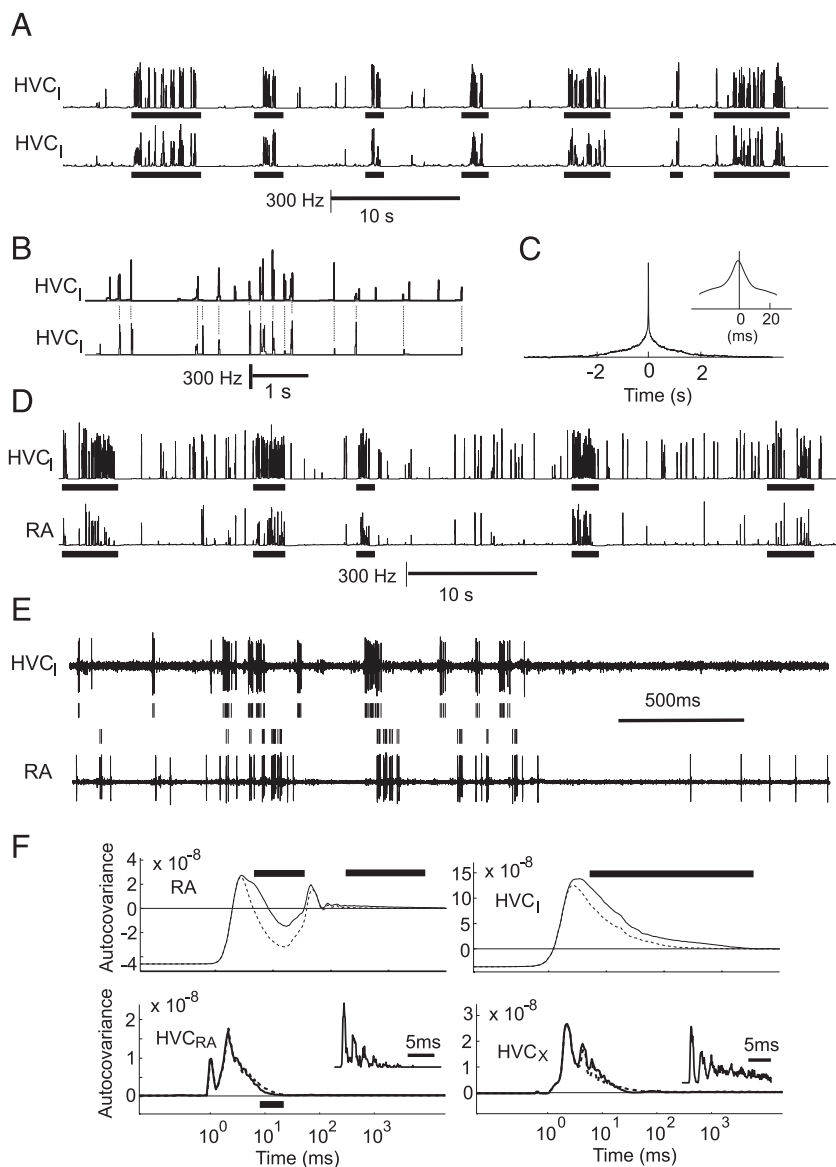


FIG. 5. Complex activity patterns on short and long time scales. *A* and *B*: instantaneous firing rate functions of simultaneously recorded  $HVC_1$  neurons. In *A*, epochs of increased bursting (thick horizontal bars) tended to occur simultaneously in the 2 neurons. In *B*, on a smaller time scale, nearly every burst in 1  $HVC_1$  neuron was associated with a simultaneous burst in the other  $HVC_1$  neuron. *C*: cross-covariance function for this neuron pair decayed to 0 only after  $>1$  s, indicating the typical duration of burst epochs. *D*: paired recording of an  $HVC_1$  and an RA neuron also revealed burst epochs that tended to co-occur in the 2 neurons. *E*: raw extracellular spike waveforms of an  $HVC_1$  neuron (*top*) simultaneously recorded with an RA neuron (*bottom*). In the middle, burst trains for the 2 neurons are shown after removal of single spikes. *F*: average auto-covariance functions of identified HVC and RA neurons compared with renewal functions (dashed lines). Auto-covariances are significantly larger than the renewal functions when the thick horizontal bars are plotted above the auto-covariance functions (RA and  $HVC_1$  neurons); and auto-covariances are smaller than the renewal functions when the horizontal bars are plotted below ( $HVC_{RA}$  neurons). For RA and  $HVC_1$  neurons, the auto-covariance functions had long tails, whereas those of HVC projection neurons did not. HVC projection neurons tended to display a characteristic burst pattern that can be seen by the oscillatory shape of auto-covariance functions between 1 and 10 ms (*insets* show example auto-covariance functions from single neurons).

between the singing and waking states in RA and HVC neurons, we recalculated firing-rate histograms with restriction to burst-related firing only. To this end, we removed single spikes from the original spike trains and analyzed the resulting burst trains. The firing-rate distributions of burst trains were almost as wide as those of the original spike trains, illustrating that most periods of spiking at high rates were associated with sleep bursts (Fig. 6A, ○).

By comparing the original spike trains with burst trains, we determined the percentage of spikes that were part of a burst during sleep. This number was sleep-state dependent and was different for the different neuron types. For example, on average, for  $HVC_{RA}$  neurons,  $>70\%$  of spikes were part of a burst, whereas for RA neurons, this number was  $<20\%$ . The average burst rate of  $HVC_1$  neurons was  $>2$  bursts/s—during the short epochs of very dense bursting, this number could be as high as 10–25 bursts/s. RA neurons had an average burst rate of almost 1 burst/s with peaks as high as 5–12 bursts/s. In contrast,  $HVC_{RA}$  and  $HVC_X$  neurons produced bursts extremely rarely, on average one burst every  $\sim 10$  s. Averages of

firing rates, firing rates during bursts, burst rates, burst widths, the number of spikes per burst, and the fraction of spikes in a burst are summarized in Table 1.

To account for sleep-state-dependent variability that might have influenced burst measurements reported in Table 1, we also measured firing rates in burst trains using simultaneously recorded pairs. From these measurements, we computed the correlation coefficient of firing rates in non-overlapping 3-s windows. The result of this analysis was that the occurrence of increased bursting in one neuron of a pair tended to be positively correlated with increased bursting in the other neuron (Fig. 6B, ■, significantly correlated pairs). In all 50 RA- $HVC_1$  neuron pairs, the firing rate correlation was significant, with an average correlation coefficient of 0.66. In 38 of 47  $HVC_{RA}$ -RA neuron pairs, the firing-rate correlation of burst trains was significant as well, with an average coefficient of 0.43. In 16 of 26  $HVC_{RA}$ - $HVC_1$  neuron pairs, the correlation was significant, with an average coefficient of 0.47. A similar picture also emerges for the  $HVC_X$  neurons. They exhibited significant correla-

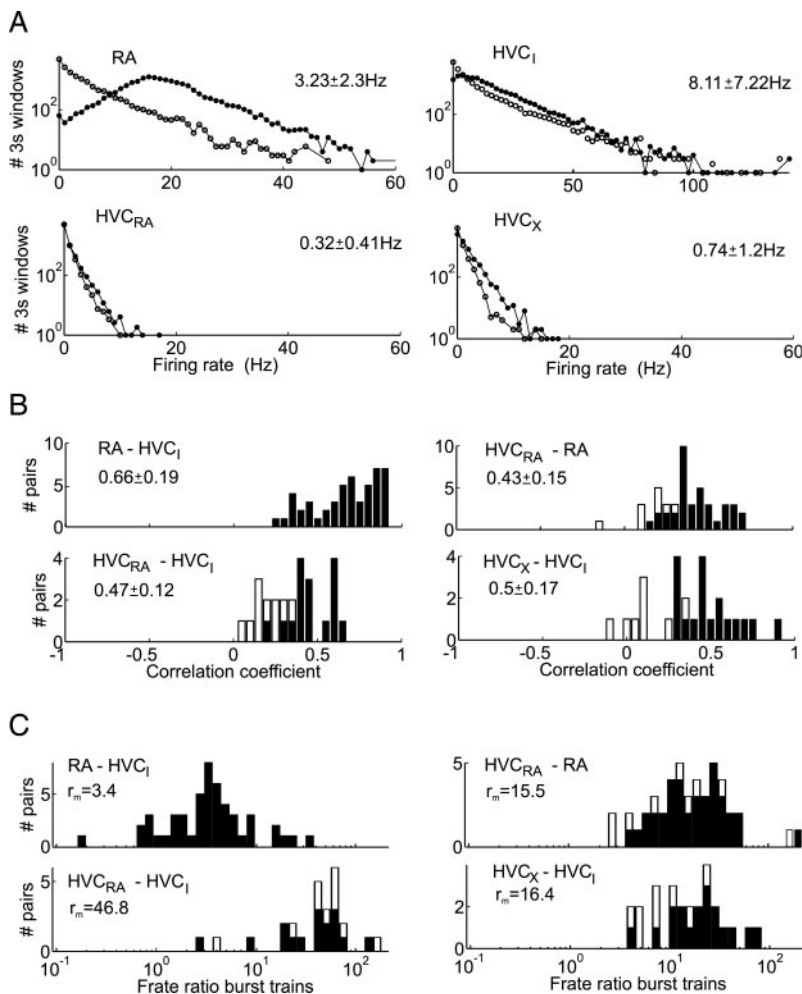


FIG. 6. Firing rates in RA,  $HVC_{RA}$ ,  $HVC_I$ , and  $HVC_X$  neurons, measured in 3-s windows. **A**: firing rate distributions from single neuron recordings. ●, average firing rates in regular spike trains; ○, firing rates from burst trains with single spikes removed. The numbers shown (*top right*) are average firing rates and SDs for the burst trains. Firing rate distributions of RA neurons had the strongest dependence on nonburst spikes. **B**: correlation coefficients derived from burst trains in different neuron types. ■, significantly correlated pairs ( $P < 0.05$ ); □, insignificantly correlated ones. The numbers represent averages  $\pm$  SDs of measured correlation coefficients. As can be seen, nearly all recorded neuron pairs displayed significantly and positively correlated firing rates. **C**: firing-rate ratios for significantly correlated pairs (■) and remaining pairs (□). The numbers labeled  $r_m$  are median firing-rate (Frate) ratios. Typically, firing-rate ratios for a given neuron type were dispersed over  $>1$  order of magnitude.

tions in 18 of 26 paired recording with  $HVC_I$  neurons, resulting in an average coefficient of 0.5.

As we have seen in Fig. 6A, the firing rates in burst trains were widely distributed. We also observed a wide distribution for the firing-rate ratios in simultaneously recorded neuron pairs, Fig. 6C. Typically, these ratios were  $\sim 50\%$  larger than the ratios inferred from single neuron recordings (Table 1, *last column*). Due to insensitivity to sleep nonstationarities, we believe the estimated ratios from paired recordings to be more accurate than the single neuron estimates. A simple self-consistency test reinforced us in this belief: By multiplying the median firing rate ratio of  $HVC_{RA}$ -RA pairs (15.5) with the median ratio of RA- $HVC_I$  pairs (3.4), we obtained a value of 52.7, which was close to the measured ratio of  $HVC_{RA}$ - $HVC_I$  pairs of 46.8.

We also used our paired recordings to estimate burst rate ratios (number of bursts per second, see METHODS). We found that RA neurons burst 13.9 times as often as did  $HVC_{RA}$  neurons, and  $HVC_I$  neurons burst 2.7 times as often as did RA neurons. These data imply that  $HVC_I$  neurons should burst roughly 37.5 times as often as do  $HVC_{RA}$  neurons, a number that is close to our measured value of 32.6. Note that the burst-rate ratio of RA neurons and  $HVC_{RA}$  neurons of 13.9 is very similar to that found during singing [ $\sim 12$  bursts per motif for RA neurons (Leonardo and Fee 2005) and 1 burst per motif for  $HVC_{RA}$  neurons (Hahnloser et al. 2002)].

#### Analysis of burst patterns in the premotor pathway

By creating raster plots of RA neuron activity, time-aligned to the onset of bursts in  $HVC_{RA}$  neurons, we frequently observed correlated patterns of spikes (Fig. 7A). As previously reported, RA neurons nearly always exhibit a brief sequence of bursts reliably locked to the sparse  $HVC_{RA}$  neuron bursts (Hahnloser et al. 2002). Although well correlated to the  $HVC_{RA}$  bursts, the bursts in RA neurons were generally not synchronized (at 0 time lag) but occurred over a wide range of time lags relative to the bursts of  $HVC_{RA}$  neurons. We have quantified the correlated spike events by the coherency function (see METHODS). Most  $HVC_{RA}$ -RA neuron pairs exhibited at least one significant coherency peak (35/46 pairs had  $\geq 1$  significant peak, among which 21 pairs had exactly 1 significant peak, 12 pairs had 2 peaks, 1 pair had 3 peaks, and 1 pair had 4 peaks). Main peaks had a median time lag relative to  $HVC_{RA}$  neuron spikes of 6 ms, in the range from  $-63$  to 65 ms, Fig. 8A, *bottom*. All peaks including secondary peaks were dispersed over a range from about  $-80$  to 110 ms. The average coherency function of  $HVC_{RA}$ -RA neuron pairs exhibited a peak value of  $3 \times 10^{-3}$  at a time lag of 6 ms relative to the  $HVC_{RA}$  neuron spikes, Fig. 8A, *top*. As can be seen, this peak value was above the average significance threshold for  $HVC_{RA}$  and RA neurons (Fig. 8A). These results agree with the causal notion that  $HVC_{RA}$  neurons drive spikes in RA neurons at a

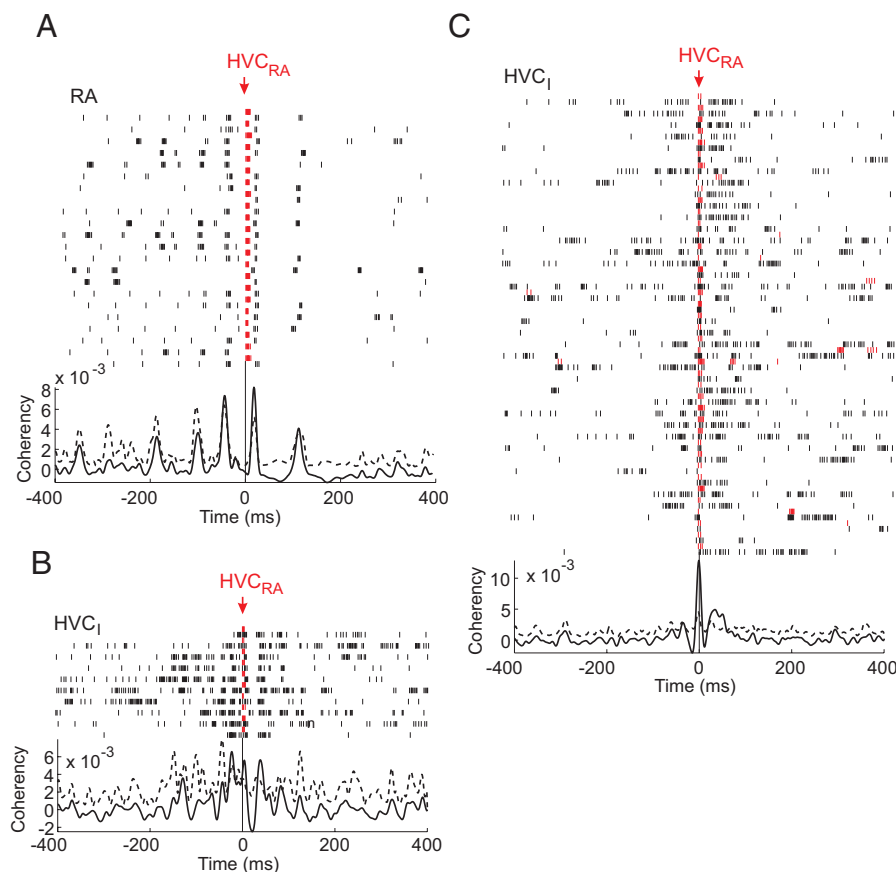


FIG. 7. Spike raster plots and coherency functions of paired recordings of  $HVC_{RA}$  neurons with RA or  $HVC_1$  neurons. *A*: spike trains of RA neurons were aligned to bursts in a simultaneously recorded  $HVC_{RA}$  neuron.  $HVC_{RA}$  bursts (short red rasters) were aligned on the 1st spike at the center of the plot. Corresponding RA spikes are shown below each  $HVC_{RA}$  burst (long black dots). Note the reproducible pattern of RA bursts associated with  $HVC_{RA}$  bursts. Below each raster plot is the coherency function plotted as a black line with the significance threshold shown by the dashed line. Only at time lags where the black line exceeds the dashed line is the coherency between these neurons significant. *B* and *C*: raster plots of simultaneously recorded  $HVC_{RA}$ - $HVC_1$  neuron pairs, aligned to the onsets of  $HVC_{RA}$  neuron bursts. In both cases, increased spiking of the  $HVC_1$  neuron is visible near  $HVC_{RA}$  neuron bursts.

time lag within the range of measured spike latencies in Fig. 3C.

Nearly all  $HVC_1$  neurons we recorded were antidromically activated from RA, confirming previous findings that they receive strong excitatory synaptic input from  $HVC_{RA}$  neurons (Mooney and Prather 2005; Rosen and Mooney 2003). In paired recordings, we found that  $HVC_1$  neurons exhibited small periods of dense bursting, time-locked to  $HVC_{RA}$  neuron bursts, Fig. 7, *B* and *C*.

The coherency functions and peaks between different HVC and RA neuron types are summarized in Fig. 8. The average coherency function of RA neuron pairs peaked at 0 ms, with a peak coherency of  $9 \times 10^{-3}$ , Fig. 8*B*, *top*. Of 31 recorded RA neuron pairs, 26 exhibited at least one significant coherency peak. Main peaks were narrowly distributed in the time interval from  $-10$  to  $8$  ms (excluding 1 outlier at  $-140$  ms). The average coherency function between RA and  $HVC_1$  neurons reached a peak of  $1.4 \times 10^{-2}$  at a time lag of  $-4$  ms (Fig. 8*E*, *top*), indicating that  $HVC_1$  neurons tended to spike shortly before RA neurons did. All of 50 recorded RA- $HVC_1$  neuron pairs exhibited at least one significant (and central) coherency peak. Main peaks were distributed over an interval from  $-9$  to  $11$  ms, with a median peak time lag of  $-2$  ms, Fig. 8*E*, *bottom*. The average coherency function of  $HVC_{RA}$ - $HVC_1$  neuron pairs peaked at a time lag of 0 ms with a peak value of  $7 \times 10^{-3}$ , Fig. 8*C*, *top*. In 23 of 26 recorded pairs, we found at least one significant coherency peak. Main peaks were widely distributed, from  $-28$  to  $17$  ms, with a median peak time lag of 1 ms Fig. 8*C*, *bottom*. Finally, the average coherency function of  $HVC_1$  neuron pairs reached a large peak value of  $3.9 \times 10^{-2}$ ,

Fig. 8*D*, *top*. All of the 19 recorded neuron pairs exhibited at least one significant coherency peak. Central peaks were narrowly distributed, from just  $-5$  to  $4$  ms, Fig. 8*D*, *bottom*.

The large range of time lags of coherency peaks between  $HVC_{RA}$  and RA neurons in Fig. 8*A* prevented us from precisely estimating the latency of HVC drive to RA. However, given the 0 ms time lag of the average  $HVC_{RA}$ - $HVC_1$  coherency function (Fig. 8*C*, *top*) and the  $-4$  ms time lag of the average RA- $HVC_1$  coherency function (Fig. 8*E*, *top*), we inferred a roughly  $4 \pm 0.5$ -ms latency of the  $HVC_{RA}$  neuron drive to RA neurons (the SE of 0.5 ms was estimated by the SD of 2.3 ms for the central peaks between the 26  $HVC_1$ -RA neuron pairs and an estimated SD of 1.0 ms for the 0-ms time lag of the average  $HVC_{RA}$ - $HVC_1$  coherency). Thus we found that the inferred latency of  $HVC_{RA}$  neuron drive to RA neurons agreed well with the average  $HVC_{RA}$  antidromic spike latency of 4.6 ms shown in Fig. 3C.

In conclusion, between HVC and RA neurons we find highly significant spike coherencies that peak at time lags consistent with a causal role of HVC neurons driving spikes in RA neurons.

#### Activity in the anterior forebrain pathway (AFP)

We examined the AFP for a possible role in the generation of RA burst sequences. First we studied the HVC input to the AFP by performing paired recordings of  $HVC_X$  neurons with other HVC neuron types. Raster plots revealed correlations between  $HVC_X$  and  $HVC_1$  neurons, an example is shown in Fig. 9*A*. The average coherency function between  $HVC_X$  and

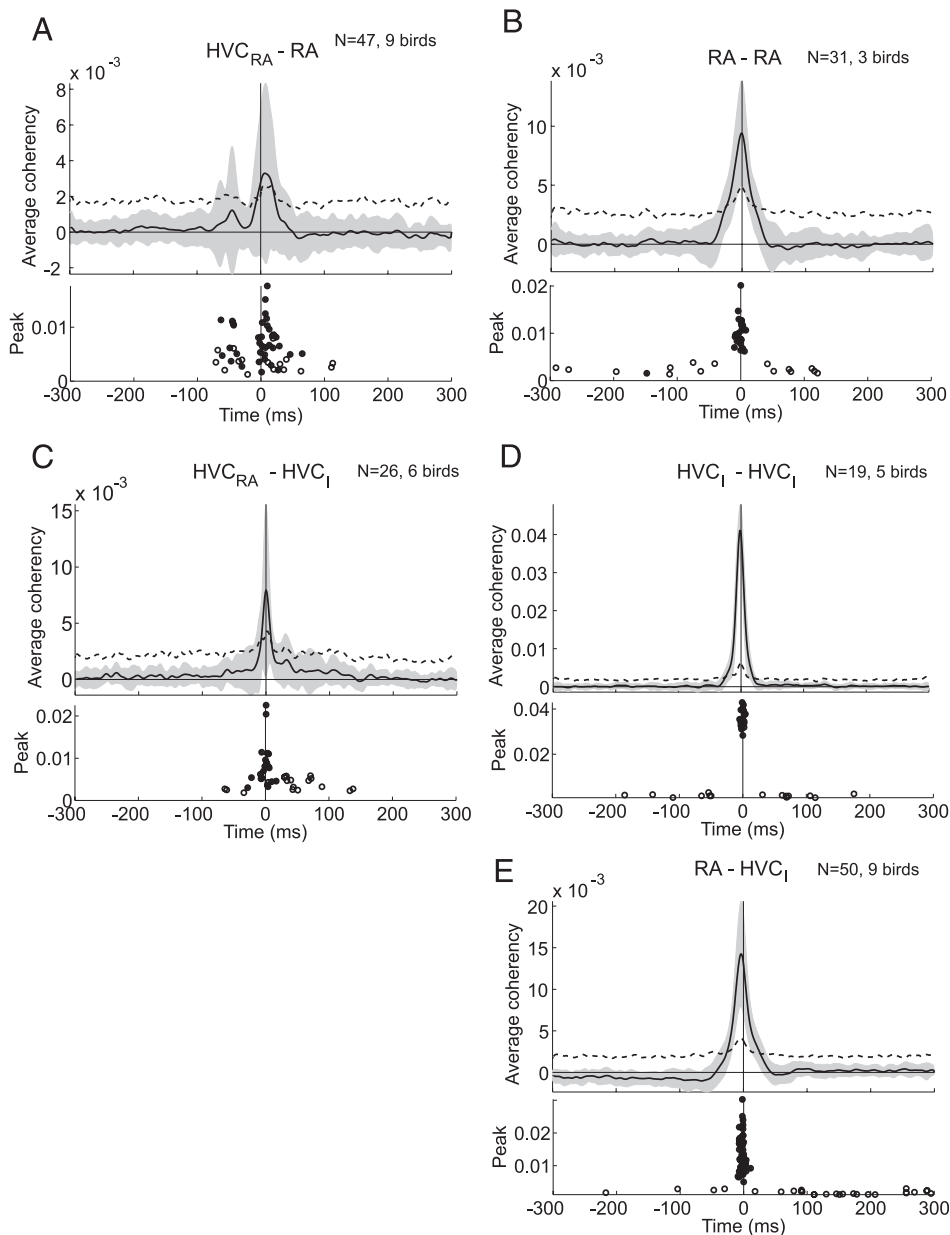


FIG. 8. Average coherency functions and distribution of coherency peaks for different neuron types. *Top part* of each subplot is the average coherency function between all neuron pairs (—) and the average significance threshold (---).  $\square$ , SD of coherency functions. In the *bottom parts*, the peaks of individual coherency functions are shown.  $\bullet$ , main peaks of individual neuron pairs;  $\circ$ , significant secondary peaks (of smaller coherency value than the main peaks). There is usually a broad peak close to 0 time lag at which the average coherency was well above the average significance threshold. A:  $HVC_{RA}$ -RA neurons; B: RA-RA neurons; C:  $HVC_{RA}$ - $HVC_I$  neurons; D:  $HVC_I$ - $HVC_I$  neurons; E: RA- $HVC_I$  neurons.

$HVC_I$  neurons exhibited a significant peak of  $5 \cdot 10^{-3}$  at a time lag of 1.3 ms, Fig. 9B, *top*. Accordingly,  $HVC_X$  neurons tended to spike before  $HVC_I$  neurons did. Of 26 recorded  $HVC_X$ - $HVC_I$  neuron pairs, 17 exhibited at least one significant coherency peak. Main coherency peaks ranged from  $-18$  to 26 ms (excluding 3 outliers), with a median peak time lag of 4 ms, Fig. 9B, *bottom*. In summary,  $HVC_X$  neurons were less correlated with  $HVC_I$  neurons than were the  $HVC_{RA}$  neurons.

The synchrony of  $HVC_X$  neurons with  $HVC_I$  neurons suggests that  $HVC_X$  neurons engage in the sparse  $HVC_{RA}$  neuron sequences. The reason for this suggestion is that correlations of random variable pairs X and Y, and Y and Z, usually imply that X and Z are correlated as well. In seven paired recordings in three birds of  $HVC_X$  and  $HVC_{RA}$  neurons, we found one pair that showed strongly correlated activity, Fig. 9C: the  $HVC_X$  neuron tended to burst reliably before the  $HVC_{RA}$  neuron did, showing that  $HVC_X$  neuron activity can be time-locked to  $HVC_{RA}$  neuron sequences. We believe the reason why we

found so few correlated  $HVC_X$ - $HVC_{RA}$  neuron pairs is the sparse activity of these neurons, making it unlikely that any two of them will fire at a small enough time lag to each other. We further tested the temporal locking of  $HVC_X$  neuron activity with  $HVC_{RA}$  neuron sequences by paired recordings from  $HVC_X$  and RA neurons. In 12 paired recordings, we found 7 pairs that exhibited at least one significant coherency peak. The average coherency function between  $HVC_X$  and RA neurons exhibited a significant peak of  $2.2 \cdot 10^{-3}$  at a time lag of 4.2 ms, indicating that  $HVC_X$  neurons tended to spike a few milliseconds before RA neurons did, Fig. 9D, *top*. Main coherency peaks ranged from  $-59$  to 19 ms with a median peak time lag of 0 ms, Fig. 9D, *bottom*. The average coherency between  $HVC_X$  neurons and RA neurons was smaller than the average coherency between  $HVC_{RA}$  and RA neurons. Nevertheless, our data show that HVC sleep sequences transmitted to Area X are qualitatively similar to the sequences sent to RA. Such a similarity has also been observed during singing, in

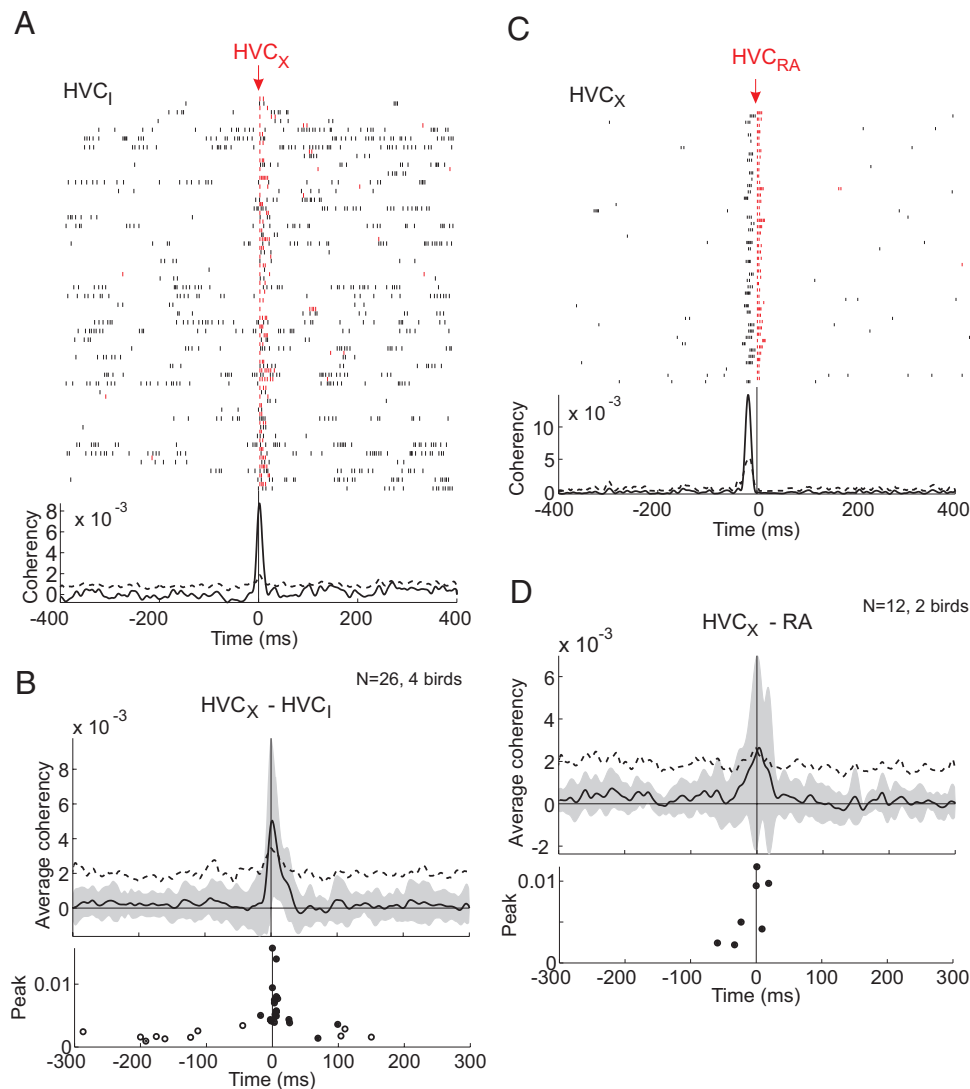


FIG. 9. HVC<sub>X</sub> neurons. *A*: raster plot of simultaneously recorded HVC<sub>X</sub>-HVC<sub>I</sub> neuron pair, aligned to the onsets of the HVC<sub>X</sub> neuron bursts. The coherency function in the bottom shows a highly significant peak at roughly 3 ms. *B*: average coherency function between HVC<sub>X</sub> and HVC<sub>I</sub> neurons. Symbols are as in Fig. 8. *C*: raster plot of HVC<sub>X</sub> neuron spikes, time-aligned to burst onsets in an HVC<sub>RA</sub> neuron, showing tight temporal locking. *D*: average coherency function between HVC<sub>X</sub> and RA neurons, showing a weakly significant peak at a small positive time lag.

which both HVC<sub>X</sub> and HVC<sub>RA</sub> neurons were found to be sparsely bursting (Hahnloser et al. 2002).

In conclusion, the coherent activity in HVC<sub>X</sub> neurons raises the question whether the correlations between HVC<sub>RA</sub> and RA neurons arise from the direct pathway between HVC and RA or from the AFP or from both.

#### Reversible HVC and LMAN lesions

To determine the relative roles of the premotor pathway and the AFP in generating sleep bursts in RA, we examined the effect of reversible inactivation of LMAN while recording activity in RA, Fig. 10. When we injected the sodium-channel blocker lidocaine into HVC, the spontaneous bursting of RA neurons immediately stopped, but recovered after ~2–3 min (pre: 1.29 bursts/s, post: 0.10 bursts/s, recovery: 1.21 bursts/s, 3/3 birds, Fig. 10, *A* and *C*). Saline injections into HVC did not have any significant effects on RA neuron burst rates ( $P < 0.01$ ,  $n = 3$  birds).

In contrast to these findings, when we injected lidocaine into LMAN, we did not observe any effects on burst rate in RA, (pre: 0.95 bursts/s, post: 1.03 bursts/s, 3/3 birds, Fig. 10, *B* and *D*). In both lidocaine injection experiments, we verified that

lidocaine did not leak into RA after the injections by recording the tonic firing of RA neurons that is otherwise typical of wakefulness. In conclusion, inactivation experiments confirmed our previous findings (Hahnloser et al. 2002) and suggest that activity in the AFP, in contrast to HVC, has little effect on RA sleep burst rate.

#### RA-projecting LMAN neurons

To investigate the relation of LMAN activity with RA activity in the sleeping adult bird, we recorded antidromically identified LMAN<sub>RA</sub> neurons. LMAN projection neurons have spinous dendrites and bifurcating axons that project to Area X and to RA (Livingston and Mooney 1997). Unlike HVC<sub>RA</sub> neurons, RA-projecting LMAN neurons (LMAN<sub>RA</sub> neurons) exhibit little firing rate adaptation in vivo to intracellular current injections (Mooney 2000; Rosen and Mooney 2000). In the singing bird, they exhibit random activity patterns and are involved in producing song variability (Kao et al. 2005; Olveczky et al. 2005). LMAN<sub>RA</sub> neurons are glutamatergic, but unlike HVC<sub>RA</sub> neurons, in the adult bird, they connect onto RA neurons exclusively via NMDA-type synaptic receptors (Mooney 1992; Stark and Perkel 1999).

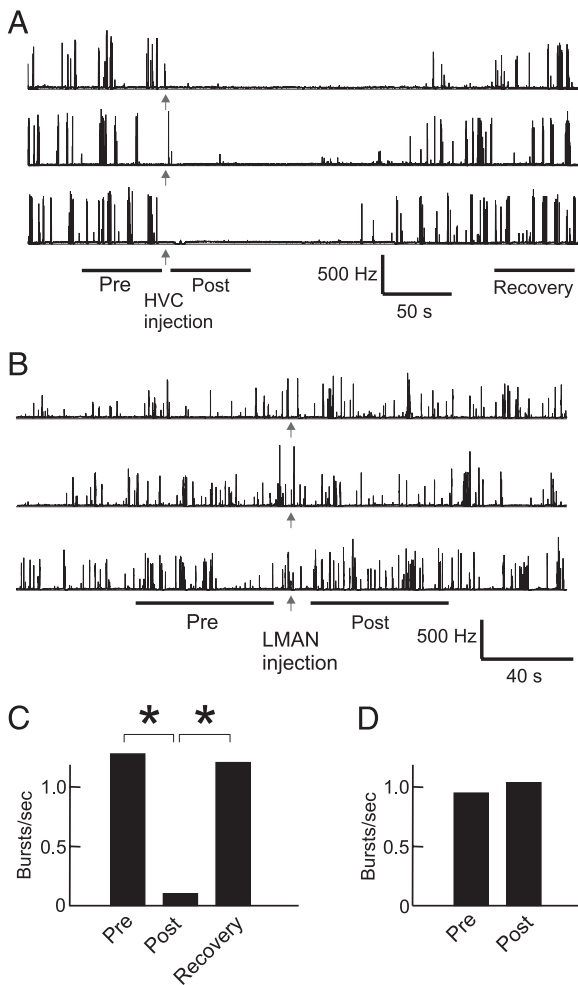


FIG. 10. Effect of lidocaine injections into HVC and LMAN on sleep burst rate in RA neurons. *A*: lidocaine injections into HVC immediately disrupted bursting in RA neurons as revealed by plots of instantaneous firing rates (the horizontal lines denote 0 Hz). Bursting recovered within 2–3 min. *B*: lidocaine injections into LMAN had no effect on RA neuron burst rate. *C*: average drop in RA neuron burst rates measured in the interval 0–60 s after the HVC injection (post) was significant when compared with burst rates before the injection (pre) and when compared with burst rates 240–300 s after the injection (recovery;  $P < 0.01$ , marked by asterisk). In *A* and *B*, the pre, post, and recovery intervals are indicated by thick horizontal bars. *D*: there was no significant change in average burst rate in RA neurons after LMAN injections. For the LMAN injections, we measured burst rates in the same pre and post intervals as for the HVC injections.

We found that electrical stimulation in RA produced antidromic spikes in LMAN of short latency ( $2.54 \pm 0.81$  ms, range: 1.6–4.7 ms, Fig. 11*A*). All neurons that responded to RA stimulation were identified by the spike collision test as LMAN<sub>RA</sub> neurons, Fig. 11*B*. LMAN neurons that did not respond to electrical stimulation in RA were excluded from further analysis. Bursts in LMAN<sub>RA</sub> neurons were rare, they had a low peak firing rate, and typically were composed of only two to three spikes. The firing properties of LMAN<sub>RA</sub> neurons are summarized in Table 1: LMAN<sub>RA</sub> burst rates were comparable to those of HVC projection neurons, though their average firing rates were roughly twice as high.

The average ISI pdf of LMAN<sub>RA</sub> neurons showed a broad peak at  $\sim 10$  ms, Fig. 11*C*. The average auto-covariance function of LMAN<sub>RA</sub> neurons peaked at short times ( $< 10$  ms) and decayed to zero only within several tens of seconds,

exhibiting the longest tail of all recorded neuron types in this study (compare Fig. 11*D* to Fig. 6). Of 29 LMAN<sub>RA</sub> neurons, all had renewal auto-covariance functions (Jackknife,  $P < 0.001$ ). Nevertheless, the median auto-covariance function of LMAN<sub>RA</sub> neurons was significantly larger than the median renewal function in the time interval 7–11 ms (Mann-Whitney rank sum test,  $P < 0.001$ ).

To investigate correlations between LMAN and RA activity, we performed paired recordings of LMAN<sub>RA</sub> and RA neurons during sleep. Figure 12*A* shows a typical example, in which the activity of the LMAN<sub>RA</sub> neuron was highly fluctuating. There is no apparent relation between LMAN<sub>RA</sub> spikes and RA neuron bursts. The average coherency function between LMAN<sub>RA</sub> and RA neurons was positive over a broad range from about  $-200$  to  $70$  ms but did not extend above the average significance threshold, Fig. 12*B*, *top*. The peak of  $1.5 \cdot 10^{-3}$  of the average coherency function was reached at a positive time lag of  $13$  ms. Of 11 recorded pairs, 8 exhibited at least one significant coherency peak. Main peaks were distributed over a large range from  $-91$  to  $27$  ms, with a median peak time lag of  $-40$  ms relative to LMAN<sub>RA</sub> neuron spikes. The largest main peak occurred at a negative time lag (Fig. 12*B*, *bottom*), indicating that in these neurons, the LMAN<sub>RA</sub> spikes were most significant when they occurred after RA neuron spikes. Further analysis showed that coherency peaks at a positive time lag in Fig. 12*B* were not very robust: by removing single spikes from both LMAN<sub>RA</sub> and RA neuron spike trains before running the coherency analysis, we found that no significant coherency peak remained at a positive time lag, suggesting that LMAN<sub>RA</sub> neuron bursts were not effective in driving bursts in RA neurons. Note, when single spikes were removed from paired recordings of HVC and RA neurons, all significant coherency peaks remained, indicating a strong causal link between bursts in HVC and RA.

To investigate correlations between LMAN and HVC activity, we performed paired recordings of LMAN<sub>RA</sub> and HVC<sub>I</sub> neurons. Again, there was a broad range over which the average coherency function was positive but without extending above the average significance threshold. Of 14 recorded LMAN<sub>RA</sub>-HVC<sub>I</sub> neuron pairs, 12 exhibited at least one significant coherency peak. Individual peak times ranged from  $-90$  to  $36$  ms with a median peak time lag of  $-27$  ms, Fig. 12*C*, *bottom*.

In conclusion, even though LMAN activity was not coherent on average at any time lag with either HVC or RA activity, individual neuron pairs exhibited significant coherency peaks distributed over a wide range of time lags. Coherency peaks in Fig. 12 were smaller than coherency peaks between HVC neurons and RA neurons in Fig. 8. Based on these results, we estimate the potential LMAN drive to RA to be significantly smaller than the HVC drive, in agreement with our reversible lesions results in Fig. 11.

#### Model: coherency peaks from serial correlations

We have found that for many neuron types, coherency functions exhibited significant peaks at both positive and negative time lags. Depending on neuron types, either the peak at positive or negative time lag is in apparent disagreement with a feedforward connection between brain areas. For example, many HVC<sub>RA</sub> neurons spiked reliably after RA neurons did

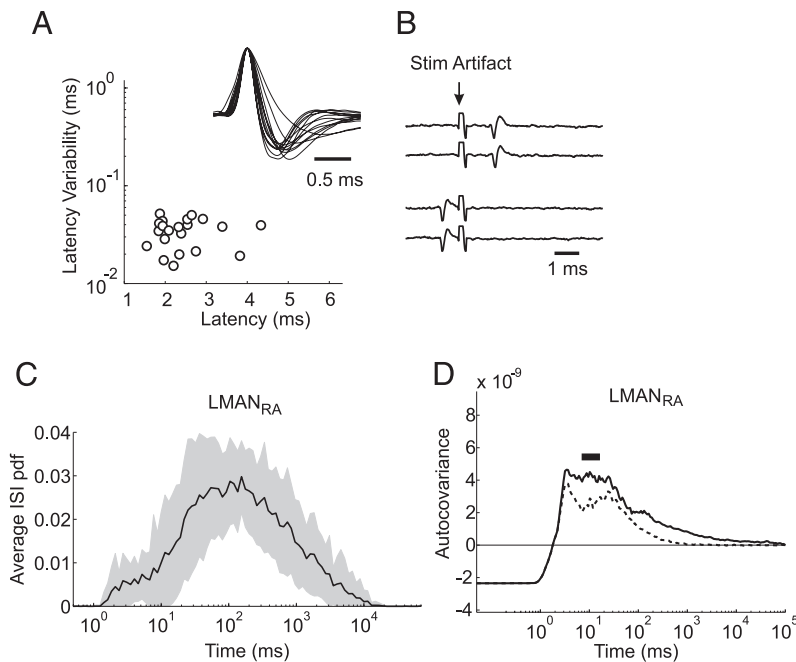


FIG. 11.  $LMAN_{RA}$  neurons. *A*: antidromic stimulation in RA activated neurons in LMAN with small latency variability ( $<0.1$  ms). *Inset*: normalized extracellular waveforms of  $LMAN_{RA}$  neurons. *B*: example collision test showing response failure of an  $LMAN_{RA}$  neuron when antidromically stimulated 1 ms after spontaneous spikes. *C*: average interspike interval probability density function of  $LMAN_{RA}$  neurons had a single broad peak. *D*: average auto-covariance function of  $LMAN_{RA}$  neurons exhibited an unusually long tail of several tens of seconds. There is a small time interval where auto-covariance functions were significantly larger than the renewal functions (thick horizontal bar).

(Fig. 8A) even though HVC projects to RA and not vice versa. Similarly, many  $LMAN_{RA}$  neurons spiked after RA neurons did (Fig. 12B), even though LMAN projects to RA and not vice versa. Finally, many  $LMAN_{RA}$  neurons spiked before  $HVC_1$  neurons did (Fig. 12C), even though the AFP extends from HVC to LMAN (via Area X and DLM) not vice versa.

With our following model we wanted to explore whether these dual coherency peaks could be seen as a byproduct of serial correlations within HVC. The underlying assumption of our model is a discrete-time, probabilistic mechanism for the

generation of HVC burst sequences. We assumed that every second, some  $HVC_{RA}$  and  $HVC_X$  neurons are stimulated from a source outside of HVC. With unit probability, the stimulated  $HVC_{RA}$  neurons respond with a burst to the external stimulation, and with probability 0.8, the stimulated  $HVC_X$  neurons respond with a burst. If and only if  $HVC_X$  neurons burst, then a HVC bursts sequence (or epoch) is initiated. Forty milliseconds later, the sequence may either stop or proceed for another 40 ms (with probability 0.8). This process is repeated in discrete time intervals of 40 ms until the stimulated  $HVC_X$

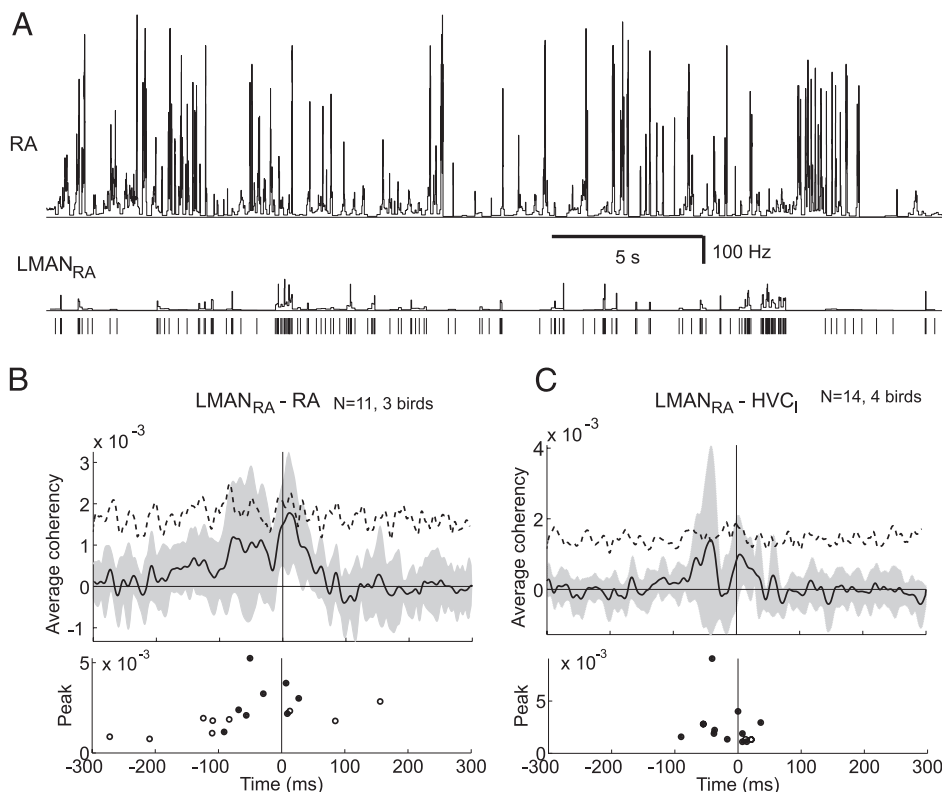


FIG. 12. *A*: example paired recording of an  $LMAN_{RA}$  and an RA neuron. There is no visually obvious correlation between the  $LMAN_{RA}$  neuron spikes and the RA neuron bursts. Below the instantaneous firing rate of the  $LMAN_{RA}$  neuron, we have also plotted its spike train for better visibility of the single spikes. *B*: average  $LMAN_{RA}$ -RA coherency function did not exceed the significance threshold (top). The significant coherency peaks of individual pairs were broadly scattered around zero time lag. *C*: similar result applied to the average  $LMAN_{RA}$ - $HVC_1$  coherency function and the distribution of significant peaks.

neurons fail to burst and the sequence comes to a halt. In other terms, we modeled HVC activity by a Markov chain such that bursts are expressed as probabilistic events, and long activity sequences are less frequent than short ones.

For simplicity, we did not model the HVC burst sequence in continuous time. We restricted our simulations of sequence dynamics to bifurcation events separated by 40-ms intervals (see METHODS). Bursts in the various HVC, RA, and LMAN neurons were modeled at fixed time lags of these bifurcation events. HVC neuron bursts had a zero time lag, the RA neuron bursts had a time lag of 4 ms, and the LMAN<sub>RA</sub> neuron bursts had a time lag of 40 ms. A schematic of the model is shown in Fig. 13A.

Spike trains from a Monte-Carlo simulation of this model are shown on a large and on a small time scale in Fig. 13, B and C, respectively. Spike trains were generated by randomly selecting a small number of ISIs for each of the burst events, giving rise to fluctuating instantaneous firing rates. The spike trains of the HVC<sub>X</sub> and HVC<sub>RA</sub> neurons were produced by considering different states in the HVC sequence, assuming that HVC projection neurons burst at most once per burst epoch. In the simulations, for each burst epoch, we associated the HVC<sub>X</sub> and HVC<sub>RA</sub> neurons with a randomly selected bifurcation event. For example, in Fig. 13B, the HVC<sub>X</sub> neuron

was not bursting in the first two burst epochs. Then in the third burst epoch it was part of the first bifurcation event, and in the fourth epoch it was part of the seventh event, etc.

Average coherency functions for these spike trains shown in Fig. 13D were in good agreement with the measured ones in Figs. 8A and 12, B and C. There was a single large coherency peak between the RA and the HVC<sub>1</sub> neuron centered at -4 ms. The coherency function of the HVC<sub>RA</sub>-RA neuron pair had a main peak at 4 ms and smaller peaks 40 ms apart, both at positive and negative time lags. The two coherency functions involving the LMAN<sub>RA</sub> neuron clearly exhibited two main peaks, one at a negative time lag and one at a positive time lag. The location of these two peaks was quite sensitive on simulation parameters. Their location was only as shown if the burst probability of HVC<sub>X</sub> neurons was smaller than that of HVC<sub>RA</sub> neurons (0.8 vs. 1). Additional simulations showed that in the converse case, the peak close to zero time lag disappeared in favor of a peak at -80 ms; and, in the case of equal probabilities, the LMAN<sub>RA</sub> coherency functions were symmetrical around a peak at -40 ms. The observation that coherency functions of the model were consistent with the data only if HVC<sub>RA</sub> neurons were more reliable than HVC<sub>X</sub> neurons for sustaining HVC burst sequences is interesting. It is in agreement with the finding that HVC<sub>RA</sub> neurons are more strongly

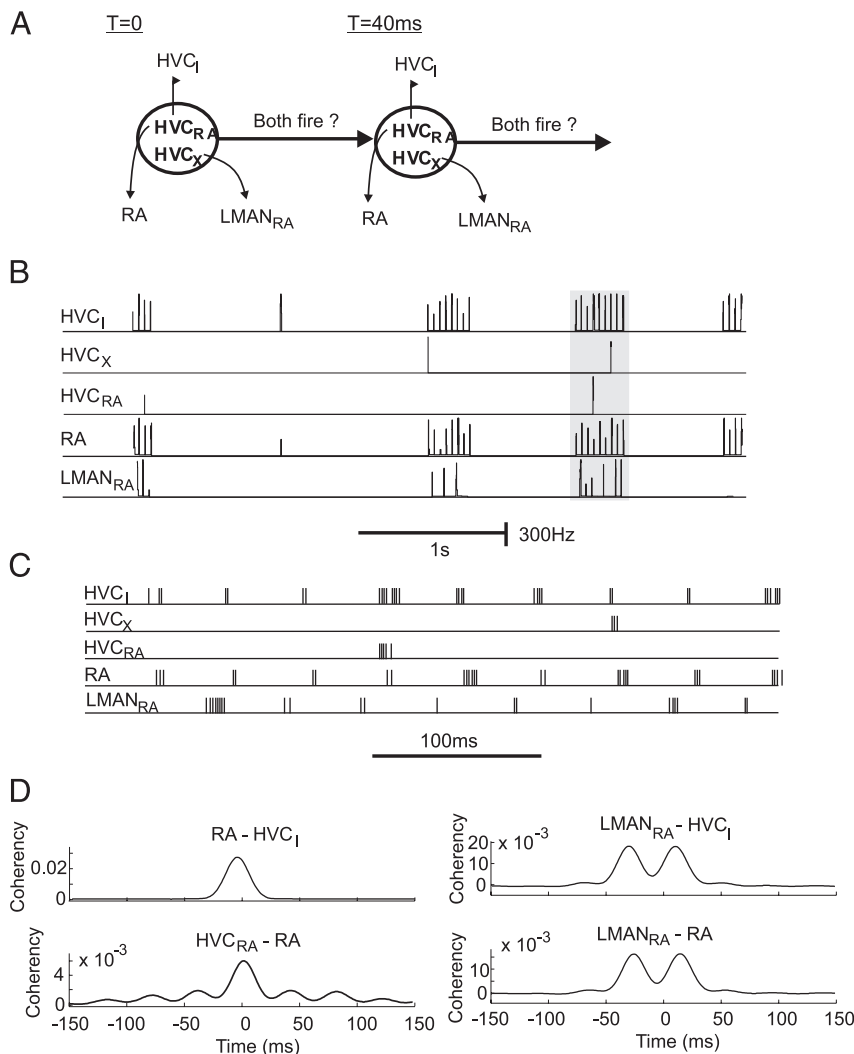


FIG. 13. Generative model of HVC, RA, and LMAN neuron spike trains. *A*: every second a probabilistic sequence of bursts is initiated in HVC. At any time, if both the HVC<sub>X</sub> and HVC<sub>RA</sub> populations fire, then the HVC sequence may progress, otherwise the sequence stops until it is reinitialized at the next second. The black arrows represent burst dependencies of other neurons in HVC, RA, and LMAN. Neuron populations are shown in bold-face, whereas single neurons in regular face. *B*: example spike trains (excerpts) generated by the model, represented as instantaneous firing rate functions. An example burst epoch is indicated by the gray area. *C*: spike trains from the burst epoch marked by gray in *B*. *D*: smoothed coherency functions and significance thresholds for the spike trains in *B*. The coherency functions of the LMAN<sub>RA</sub> neuron with RA and HVC<sub>1</sub> neurons exhibited 2 peaks due to serial correlations in HVC. By considering several HVC<sub>RA</sub> neurons in our simulation and averaging over their coherency functions with the RA neuron, several peaks emerged.

correlated with  $HVC_1$  and RA neurons than are the  $HVC_X$  neurons.

A note on our model: we chose a time interval of 40 ms between bifurcation events because of correspondence with the typical interburst interval of  $HVC_1$  neurons during dense burst epochs ( $\leq 25$  burst/s). This time interval determines the time lag between coherency peaks in Fig. 13D. We leave it open as to whether this time interval also has a mechanistic interpretation for how HVC burst sequences are generated (for example by input from Nif or Uva) or whether it can be viewed as a consequence of more complex, continuous-time simulations with stereotyped sequential behaviors (i.e., where neurons are not allowed to burst at arbitrary times in the continuous sequence but only at a fixed set of discrete times). A detailed exploration of this issue is beyond the scope of this paper.

## DISCUSSION

We set out to measure the spontaneous spike patterns and their correlations in sleeping songbirds. In particular, we examined the involvement of the premotor pathway and the anterior forebrain pathway in sleep burst generation in RA. To examine the role of inputs from HVC, we identified HVC neurons by antidromic stimulation. We found that  $HVC_1$  neuron spikes tended to be narrower than that of HVC projection neuron. However, we were unable to reliably identify HVC neuron type based on spike waveform. In a previous study of extracellular spike waveforms, it was found that  $HVC_1$  neurons could be reliably distinguished from HVC projection neurons based on their spike widths being narrower than 0.35 ms (Rauske et al. 2003). In our study, the 0.35-ms limit applied to all  $HVC_1$  neurons as well. However, it also applies to most HVC projection neurons, and so it was not a feasible criterion for neuron identification. We attribute the narrowness of projection neuron spikes in our study to the large impedances of our glass electrodes: 5–15 versus 3–5 M $\Omega$  in Rauske et al. Another reason for wider spikes in Rauske et al. might be their partial use of metal electrodes, which accentuate spike waveform differences also in our experience. Recall that the benefit of our large-impedance electrodes was our improved ability to record from  $HVC_{RA}$  neurons, which are known to have very small somata and are hard to isolate with larger electrodes.

Virtually no HVC projection neuron could be activated by stimulation in both Area X and RA. This finding suggests that  $HVC_{RA}$  and  $HVC_X$  neurons do either have very few or weak excitatory connections between them or that a possible source of synaptic excitation between these cell types is masked by fast inhibition. In support of the latter view, in recent studies of the HVC microcircuit, strong disynaptic GABAergic inhibition has been found from  $HVC_{RA}$  to  $HVC_X$  neurons (Mooney and Prather 2005; Rosen and Mooney 2003). We have found  $HVC_1$  neurons to be more reliably activated by RA stimulation than by Area X stimulation. This agrees with the finding that very few  $HVC_X$ - $HVC_1$  neuron pairs show signs of excitatory connections (Mooney and Prather 2005). In agreement with the idea that the excitatory synaptic drive from  $HVC_{RA}$  to  $HVC_1$  neurons is stronger than that of  $HVC_X$  to  $HVC_1$  neurons, we found that  $HVC_1$  neurons exhibited significant coherencies more frequently with  $HVC_{RA}$  neurons than with  $HVC_X$  neurons. Despite these possibly important differences between local  $HVC_{RA}$  and  $HVC_X$  circuits, we find qualitatively similar

sparse activity patterns in these two types of projection neurons during sleep.

Similar to previous lidocaine injection experiments where song-related auditory responses in RA were found to be mediated by HVC and not by LMAN (Doupe and Konishi 1991), we here find that LMAN is not necessary for the generation of premotor-like activity in RA: burst rates in RA are unchanged after silencing LMAN, Fig. 10.

We want to compare our results to similar studies performed in the anesthetized bird (Kimpo et al. 2003; Rauske et al. 2003). Physiological differences are known to exist between sleep and anesthesia (Cardin and Schmidt 2003). We can infer some of these differences by comparing our spontaneous firing rates in Table 1 with spontaneous rates reported in Rauske et al.:  $HVC_X$  neurons seem to have a somewhat lower spontaneous firing rate during sleep than during anesthesia (1.6 vs. 3.8 Hz), whereas  $HVC_1$  neurons seem to have a much higher firing rate during sleep ( $15.0 \pm 9.0$  vs.  $3.2 \pm 3.1$  Hz). These differences make it plausible that state dependence is an important factor that could affect spike generation mechanisms in RA.

Despite these differences, the average  $LMAN_{RA}$ -RA coherency function in Fig. 12B is qualitatively similar to coherency functions found in the anesthetized bird (Kimpo et al. 2003). Coherencies in Kimpo et al. are  $\sim 10$  times larger than the ones we depict. This apparent mismatch can be entirely attributed to our choice of bin size (1 vs. 10 ms in Kimpo et al.). To compare our measured coherency values with those in Kimpo et al. our coherency functions must be expressed in terms of 10-ms bins, which roughly amounts to multiplication by a factor of 10, resulting in good quantitative agreement.

We are able to offer a simple mechanism for our observed coherency functions. We attribute secondary coherency peaks as those in Figs. 7A, 8A, and 12, B and C, to transient locking of neural activity into stereotyped sequential patterns. Our generative model of spike train dynamics in the HVC-LMAN-RA pathways is based on sequential burst states in HVC. Interestingly, we find good qualitative agreement with the data if  $HVC_{RA}$  neurons exhibit a stronger tendency to form sequential activation than do  $HVC_X$  neurons. In agreement with this idea, adult song structure is not changed immediately after selective lesions of  $HVC_X$  neurons (Scharff et al. 2000), suggesting that  $HVC_{RA}$  neurons can produce burst sequences even in the absence of  $HVC_X$  neuron input.

In the study of Kimpo et al., it was argued that the first peak at a negative time lag of LMAN-RA coherency functions was due to common input to LMAN and RA from HVC, whereas the second peak at a positive time lag was attributed to  $LMAN_{RA}$  neurons driving spiking activity in RA. In our model, coherency peaks at both positive and negative time lags arise from mere existence of a common source to RA and LMAN with serial correlations. Our model was not meant to provide a detailed account for the data, even though qualitative agreement was quite simple to achieve. In a sense, our model illustrates the well-known limitation of inferring cause from correlations. We did not make use of anatomical connections between  $LMAN_{RA}$  and RA neurons. The RA and LMAN burst dynamics in our model are conditionally independent, illustrating that no connections between LMAN and RA are necessary to explain dual coherency peaks in paired recordings in these areas. Finally, we would like to emphasize that our model is

only a caricature of sleep dynamics and has several shortcomings. For example, single-neuron statistics (e.g., ISI pdfs and auto-covariance functions) are only poorly reproduced. More involved models and more realistic assumptions on HVC dynamics will be necessary for a better understanding of mechanisms for spike trains generation in different neuron types. The vast diversity of burst rates and the complexity of spontaneous activity patterns make the sleeping bird an ideal system for exploring biophysical models of population activity in neural circuits.

The AFP is known to have an important role in motor learning and song maintenance. However, a detailed understanding of whether this role unfolds in an on-line mode during singing or an off-line mode during sleep is still unknown. The fact that deafening has little effect on LMAN activity during singing (Hessler and Doupe 1999) and the lack of auditory responsiveness of LMAN neurons during singing (Leonardo 2002) suggests that if LMAN plays a role in transmitting an error-related signal to the motor system, this does not occur during singing—at least in adult birds. This raises the possibility that such processing may occur during sleep. For example, it has been proposed that LMAN activity during sleep may represent a prediction of real auditory feedback—a virtual error signal (Dave and Margoliash 2000). Our recordings were made in adult birds with a crystallized song, thus any error-related activity in LMAN is likely to be small. It would be interesting to investigate whether LMAN activity exhibits strong correlations to RA bursts in birds that are actively learning their song, for example in juveniles or decrystallized adult birds (Leonardo and Konishi 1999).

From our study, we conclude that spontaneous activity in the HVC-RA circuit of adult birds during sleep is generated by essentially the same mechanism as during singing. It is currently unclear how this finding fits into theories of memory consolidation during slow-wave sleep, where usually a dramatic difference between circuit dynamics during behavior and sleep is observed (Nadasdy et al. 1999). Possibly, further experiments in juveniles or new computational ideas are needed to resolve this conundrum.

#### ACKNOWLEDGMENTS

For discussions on avian sleep physiology, we thank I. Tobler.

#### GRANTS

R.H.R. Hahnloser acknowledges support by the Swiss National Science Foundation and M. S. Fee acknowledges support from the National Science Foundation.

#### REFERENCES

- Abarbanel HDI, Gibb L, Mindlin GB, Rabinovich MI, and Talathi S. Spike timing and synaptic plasticity in the premotor pathway of birdsong. *Biol Cybern* 91: 159–167, 2004.
- Amlaner CJ Jr and Ball NJ (Editors). *Avian Sleep* (2nd ed.). Philadelphia, PA: Saunders, 1994.
- Bottjer SW, Miesner EA, and Arnold AP. Forebrain lesions disrupt development but not maintenance of song in passerine birds. *Science* 224: 901–903, 1984.
- Cardin JA and Schmidt MF. Song system auditory responses are stable and highly tuned during sedation, rapidly modulated and unselective during wakefulness, and suppressed by arousal. *J Neurophysiol* 90: 2884–2899, 2003.
- Cox DR. *Renewal Theory*. London: Mehtuen, 1962.
- Dave AS and Margoliash D. Song replay during sleep and computational rules for sensorimotor vocal learning. *Science* 290: 812–816, 2000.
- Deregnacourt S, Mitra PP, Feher O, Pythe C, and Tchernichovski O. How sleep affects the developmental learning of bird song. *Nature* 433: 710–716, 2005.
- Doupe AJ. A neural circuit specialized for vocal learning. *Curr Opin Neurobiol* 116: 104–111, 1993.
- Doupe AJ and Konishi M. Song-selective auditory circuits in the vocal control system of the zebra finch. *Proc Natl Acad Sci USA* 88: 11339–11343, 1991.
- Doupe AJ, Solis MM, Kimpo RR, and Boettiger CA. Cellular, circuit, and synaptic mechanisms in song learning. *Ann NY Acad Sci* 1016: 495–523, 2004.
- Dutar P, Vu HM, and Perkel DJ. Multiple cell types distinguished by physiological, pharmacological, and anatomic properties in nucleus HVC of the adult zebra finch. *J Neurophysiol* 80: 1828–1838, 1998.
- Fee MS, Kozhevnikov AA, and Hahnloser RH. Neural mechanisms of vocal sequence generation in the songbird. *Ann NY Acad Sci* 1016: 153–170, 2004.
- Gerstner W and Kistler W. *Spiking Neuron Models. Single Neurons, Populations, Plasticity*. Cambridge, UK: Cambridge Univ. Press, 2002.
- Hahnloser R, Kozhevnikov A, and Fee MS. An ultrasparsely code underlies the generation of neural sequences in a songbird. *Nature* 419: 65–70, 2002.
- Hessler NA and Doupe AJ. Singing-related neural activity in a dorsal forebrain-basal ganglia circuit of adult zebra finches. *J Neuroscience* 19: 10461–10481, 1999.
- Hishikawa Y, Cramer H, and Kuhlo W. Natural and melatonin-induced sleep in you chickens—a behavioral and electrographic study. *Exp Brain Res* 7: 84–94, 1969.
- Holden AV. Signal processing: neural coding by correlation? *Nature* 428:382, 2004.
- Kao MH, Doupe AJ, and Brainard MS. Contributions of an avian basal ganglia-forebrain circuit to real-time modulation of song. *Nature* 433: 638–643, 2005.
- Kimpo RR, Theunissen FE, and Doupe AJ. Propagation of correlated activity through multiple stages of a neural circuit. *J Neuroscience* 23: 5750–5761, 2003.
- Kubota M and Taniguchi I. Electrophysiological characteristics of classes of neurons in the HVC of the zebra finch. *J Neurophysiol* 80: 914–923, 1998.
- Leonardo A. Neural dynamics underlying complex behavior in a songbird. In: *Computation and Neural Systems*. Pasadena CA: Caltech, 2002.
- Leonardo A and Fee MS. Ensemble coding of vocal control in birdsong. *J Neuroscience* 19: 652–661, 2005.
- Leonardo A and Konishi M. Decrystallization of adult birdsong by perturbation of auditory feedback. *Nature* 399: 466–470, 1999.
- Livingston FS and Mooney R. Development of intrinsic and synaptic properties in a forebrain nucleus essential to avian song learning. *J Neurosci* 17: 8997–9009, 1997.
- Louie Ka and Wilson MA. Temporally structured replay of awake hippocampal ensemble activity during rapid eye movement sleep. *Neuron* 29: 145–156, 2001.
- Margoliash D. Song learning and sleep. *Nat Neurosci* 8: 546–548, 2005.
- Mooney R. Synaptic basis for developmental plasticity in a birdsong nucleus. *J Neurosci* 12: 2464–2477, 1992.
- Mooney R. Different subthreshold mechanisms underlie song selectivity in identified HVC neurons of the zebra finch. *J Neurosci* 201: 5420–5436, 2000.
- Mooney R and Prather JF. The HVC microcircuit: the synaptic basis for interactions between song motor and vocal plasticity pathways. *J Neurosci* 25: 1952–1964, 2005.
- Nadasdy Z, Hirase H, Czurko A, Csicsvari J, and Buzsaki G. Replay and time compression of recurring spike sequences in the hippocampus. *J Neurosci* 19: 9497–9507, 1999.
- Nick TA and Konishi M. Dynamic control of auditory activity during sleep: correlation between song response and EEG. *Proc Natl Acad Sci USA* 98: 14012–14016, 2001.
- Nottebohm F, Kelley DB, and Paton JA. Connections of vocal control nuclei in the canary telencephalon. *J Comp Neurol* 207: 344–357, 1982.
- Nottebohm F, Stokes TM, and Leonard CM. Central control of song in the canary, *Serinus canarius*. *J Comp Neurol* 165: 457–486, 1976.
- Okuhata S and Saito N. Synaptic connections of thalamo-cerebral vocal nuclei of the canary. *Brain Res Bull* 18: 35–44, 1987.
- Olviczky BP, Andalman AS, and Fee MS. Vocal experimentation in the juvenile songbird requires a basal ganglia circuit. *PLoS Biol* 3: e153, 2005.

- Phillips NH and Berger RJ.** Melatonin infusions restore sleep suppressed by continuous bright light in pigeons. *Neurosci Lett* 145: 217–220, 1992.
- Rauske PL, Shea SD, and Margoliash D.** State and neuronal class-dependent reconfiguration in the avian song system. *J Neurophysiol* 89: 1688–1701, 2003.
- Rosen MJ and Mooney R.** Intrinsic and extrinsic contributions to auditory selectivity in a song nucleus critical for vocal plasticity. *J Neurosci* 20: 5437–5448, 2000.
- Rosen MJ and Mooney R.** Inhibitory and excitatory mechanisms underlying auditory responses to learned vocalizations in the songbird nucleus HVC. *Neuron* 39: 177–194, 2003.
- Scharff C and Nottebohm F.** A comparative study of the behavioral deficits following lesions of various parts of the zebra finch song system: implications for vocal learning. *J Neurosci* 11: 2896–2913, 1991.
- Scharff C, Kirn JR, Grossman M, Macklis JD, and Nottebohm F.** Targeted neuronal death affects neuronal replacement and vocal behavior in adult songbirds. *Neuron* 25: 481–492, 2000.
- Sohrabji F, Nordeen EJ, and Nordeen KW.** Selective impairment of song learning following lesions of a forebrain nucleus in the juvenile zebra finch. *Behav Neural Biol* 53: 51–63, 1990.
- Stark LL and Perkel DJ.** Two-stage, input-specific synaptic maturation in a nucleus essential for vocal production in the zebra finch. *J Neurosci* 19: 9107–9116, 1999.
- Swadlow H.** Neocortical efferent neurons with very slowly conducting axons: strategies for reliable antidromic identification. *J Neurosci Methods* 79: 131–141, 1998.
- Thomson DJ and Chave AD** (Editors). *Jackknifed Error Estimates for Spectra, Coherences, and Transfer Functions*. Englewood Cliffs, NJ: Prentice Hall, 1991.
- Tobler I and Borbely AA.** Sleep and EEG spectra in the pigeon (*Columba livia*) under baseline conditions and after sleep deprivation. *J Comp Physiol [A]* 163: 729–738, 1988.
- Vicario DS and Nottebohm F.** Organization of the zebra finch song control system. I. Representation of syringeal muscles in the hypoglossal nucleus. *J Comp Neurol* 271: 346–354, 1988.
- Wilson MA and McNaughton BL.** Reactivation of hippocampal ensemble memories during sleep. *Science* 265: 676–679, 1994.
- Yu AC and Margoliash D.** Temporal hierarchical control of singing in birds. *Science* 273: 1871–1875, 1996.